GANIL

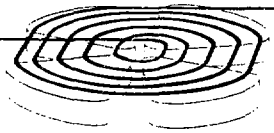

13

SOME FEATURES OF NUCLEUS-NUCLEUS COLLISIONS AT INTERMEDIATE ENERGIES

Claude Détraz, GANIL Caen, France

GANIL P. 87-19

SOME FEATURES OF NUCLEUS-NUCLEUS COLLISIONS AT INTERMEDIATE ENERGIES

Claude OETRAZ, GANIL Caen, France

Lecture presented at the International School of Physics "Enrico Fermi", Varenna, 23 June-3 July 1987.

TABLE OF CONTENTS

SOME FEATURES OF NUCLEUS-NUCLEUS COLLISIONS AT INTERMEDIATE ENERGIES

Claude DETRAZ, GANIL, Caen, France

I.- ABOUT THE SPECIFICS OF INTERMEDIATE ENERGY COLLISIONS

The so-called intermediate energies are those for which different reaction mechanisms, intrinsically incompatible, are expected to compete. Such is the case for energies ranging between 10 and 100 MeV per nucleon. The fundamental origin of the complexity expected for collisions occuring in this regime lies in the simple fact that the relative center-of-mass velocity V of the colliding nuclei is of the same order of magnitude as the average velocity v of nucleons inside the nucleus.

Both at lower and higher energies, the description of the collision can be simplified. At lower energies, the condition $V < v$ leaves time to mean-field effects to play a dominant role during the whole interaction. The dynamics of the nucleons is continuously adjusted to a varying nuclear potential, as the excitation energy and angular momentum are dissipated.

At higher energies, the opposite situation, $V > v$, does not allow the nucleons of one nucleus to feel the mean- field effects of the nucleons of the other. The reaction can be reduced to the collision of two bunches of individual nucleons whose dynamical properties are governed by the nucleus (projectile or target) to which they belong.

The mechanisms at work at low energy give their most spectacular effects in what has come to be called deep inelastic collisions, while fragmentation processes are typical of high incident energies.

None of such simplifications can be expected when $V \sim v$.

An order of magnitude of v can be derived if the nucleus is assumed to be a degenerate Fermi gas containing two varieties of Fermions. The value of the density, obtained from electron scattering experiments, $\rho = 0.17$ nucleons . fm^{-3}

leads to a value of 23 MeV for the average kinetic energy of a nucleon. Thus, intermediate energies are those for which the beam energy is not incommensurate with 23 MeV per nucleon.

That transition phenomena are expected at such an energy can also be anticipated by similar general arguments.

For instance, the wavelength λ associated with a nucleon of a projectile with an energy of say 5-10 MeV AMU^{-1}, available with major cyclotrons and tandems, is much larger than the mean distance d between two nucleons of the target nucleus. The incoming nucleon will "see" (that is, interact with) several target nucleons. The collision process will then seem to be essentially collective. In the 1960s and 70s one could thus study the fusion process, in which the two colliding nuclei fuse into a single excited nuclear system, and the so-called deep inelastic collisions, where a temporary binuclear system is formed before the two partners separate again. The latter, an unexpected process, offered significant new information on the collective properties of nuclear matter and even, at a more elementary level, on the mechanisms that allow the propagation and dissipation of energy and angular momentum.

At the other extreme, say at 1000 MeV AMU^{-1} energy, the situation is clearly the opposite, becoming smaller than d. The reaction mechanism results from the superposition of nucleon-nucleon interactions. The degree of overlap of the two colliding nuclei determines the dominant behaviour. In central collisions, complete explosion is observed, whereas in peripheral ones a participant zone, highly excited and emitting many fast nucleons, can be distinguished from the spectator zones corresponding to the non-overlapping parts of the nuclei. Despite their very low beam intensity, those high-energy machines that could accommodate heavy ions, such as the Bevalac in Berkeley and the synchrophasotron in Dubna, confirmed this overall picture.

Similarly, one can argue that the quantal nature of the colliding nuclei implies restrictions on the interaction of their nucleons. Since they are

fermions, they can only scatter into unoccupied discrete states. Because all the quantum states below the Fermi level are occupied in both nuclei, this requires that the energy available in the nucleon-nucleon collisions be large enough to promote these nucleons into highly excited states. In terms of velocity instead of energy, individual nucleon-nucleon interactions (which result in nuclear fragmentation) play a significant part in the nuclear collision only if the relative velocity of the nucleons is larger than the Fermi velocity.

This effect can probably be most clearly seen if discussed in the momentum space [1,2]. Fig. 1 shows the Fermi spheres corresponding to a uniformely filled momentum space up to the Fermi energy for three different relative velocities. The target is at left, the projectile at right. The dotted limit on the left sphere corresponds to the higher Fermi momentum associated with possible excitation of the target nucleus, up to the highest possible state assumed to be some 8 MeV above the Fermi level. At lower relative energy (10 MeV per nucleon) one observes a large overlap in the momentum space (dark area). The corresponding particles cannot be transferred from one nucleus to the other because of Pauli exclusion. Thus they transfer their whole momentum to the system, the two distinct nuclei disappear and these particles form a new nucleus through fusion. From the comparison of the three figures, one expects a disappearance of the fusion process with increasing energy.

The white areas of the two spheres correspond to momentum space occupied by nucleons of one of the two nuclei only. Thus they can freely scatter to unbound states in the other nucleus. This process can be associated with the experimental observation of preequilibrium emission of nucleons or/and direct break up (fragmentation) reactions. Its importance clearly increases with incident energy.

At last the narrow dashed zone indicates stripping reactions into bound states, i.e. a pure quasi elastic process, with cross sections expected to

become smaller when the energy increases.

Transition effects should also be expected from the following argument. The velocity of sound [3] in nuclei can be calculated from what is already known about the elementary modes of excitation of nuclear matter. The excitation energy of the giant monopole resonance is clearly related to the compressibility of nuclear matter, hence to the velocity of sound. In this way one finds that an elementary local perturbation of the wave function of nucleons propagates with a velocity of $\sim$ 30 MeV AMU^{-1}. When the relative velocity of colliding nucleons is far below this value, the perturbation induced can be distributed all over the nuclear system during collision time. In other words, thermalization can be achieved. However, for higher velocities, thermalization cannot be completed. Thus the nucleons ejected remain very energetic.

One last argument, rather trivial but certainly effective, also predicts a drastic change in reaction mechanism when the incident energy increases. It stems from the fact that the average binding energy of nucleons inside a nucleus is about 8 MeV. That means that a nucleus of mass A with inner energy larger than A x 8 MeV simply boils off. Let us assume the symmetric collision of two nuclei of mass A, with an incident energy E_0 (in MeV per nucleon) for the projectile. The total center-of-mass energy available is $\frac{1}{2} AE_0$. It must be smaller than 2 A x 8 for a complete fusion to occur. This $E_0 < 32$ MeV per nucleon is a condition for fusion. For higher incident energies, the reaction mechanism must be radically different.

It is striking that the above general arguments all lead to the conclusion that an energy of a few tens of MeV per nucleon is the limit between two different regimes of nuclear reactions. Striking, but may be not so surprising since the arguments are not completely independent : they all result from gross properties of nuclei seen in a statistical model where average velocity, average momentum, average binding energy, sound propagation are not uncorrelated. The main task of intermediate-energy heavy- ion physics

has been and still is to observe such a change in reaction mechnism and to relate the phenomena which take place at the transition with basic nuclear properties.

That a mechanism change occur proved indeed to be experimentaly spectacular. Fig. 2 represents the velocies of target fragments emitted in the collision of an ^{40}Ar beam with a ^{124}Sn target at two different energies, 27 and 44 MeV per nucleon [4].

At lower energy, peripheral and central collisions can be readily separated. The lower right peak, with heavy masses and low velocity, corresponds to transfer and break-up reactions, while the large-velocity events result from fusion reactions leading to either evaporation residues (large masses) or fission fragments (smaller masses).

The situation appears very different at 44 MeV per nucleon where a continuous evolution from quasi-elastic reactions to some incomplete fusion is observed. The well identified fusion peak observed at 27 MeV per nucleon has completely disappeared.

In the two following sections we will examine in detail the characteristics of the changing collision mechanism, particularly through the information collected during the first five years of operation of GANIL.

The GANIL energies indeed encompass the transition region where the colliding nuclei can be seen as evolving from a coherent state to a collection of individual nucleons. One can formulate it in terms of a thermo-dynamic phase transition. The nuclear system formed in low-energy collisions can be described by collective variables : it exhibits a high degree of coherence and is not unlike a liquid. The concepts of viscosity, temperature, friction and the shape parameters seem to be useful. In high-energy collisions, the system behaves like an assembly of loosely interacting individual nucleons, rather similar to a gas.

How does such a phase transition proceed and what phenomena occur when the nucleus looses its coherence ? To observe and analyse these features is

the primary experimental objective of the accelerator. More fundamentally, perhaps, these observations should allow physicists to address the following questions : out of the very large number of degrees-of-freedom of the system formed by the excited assembly of nucleons, can the few relevant parameters that describe its structure and evolution be identified ? This question defines a basic problem in statistical physics. The excited piece of nuclear matter formed in the collision has very distinctive features : it consists of a finite number of fermions, carries a high internal energy and is governed by the laws of quantum mechanics. Present-day statistical mechanics do not solve this problem, and do not provide guidelines to derive the relevant variables nor laws to describe the evolution of such a system. These answers must come from nuclear physics itself.

II.- PERIPHERAL REACTIONS

If the impact parameter could be readily measured in the course of an experiment, there would be no ambiguity in defining peripheral reactions. Of course, this is far from being the case. As will be seen, the impact parameter is determined, when possible, in an indirect and mostly model-dependent way. Yet it is an essential ingredient in the description and analysis of a collision. It has been seen consistently that what could be identified as central and peripheral collisions behaved quite differently. At this point, it will suffice to say that one will call central collisions those in which the direct trace of the projectile and/or the target nuclei is lost in the exit channel, while peripheral ones leave one of these nuclei, or both, identifiable after the collision, even if their Z or A values have been altered.

1. Fragmentation-like processes

As soon as experiments could start at GANIL, in January 1982, the observation of fast nuclei abundantly emitted forwards appeared strikingly reminiscent of the fragmentation process observed with light energy projectiles.

1.1 Experimental evidence

Figure 3, taken from ref.[5], presents a striking evidence for fragmentation at 44 MeV per nucleon. At lower incident energy, the N/Z ratio has had time to be equilibrated, so that the Si fragments emitted are neutron-rich. At higher energy, here at 213 MeV per nucleon, as observed at Bevalac [6], the N/Z of the fragment simply reflects the N/Z value of the projectile. The GANIL results of fig. 3, at 44 MeV per nucleon, are clearly consistent with the Bevalac ones. This indicates that, at intermediate energy, one already deals with the high-energy regime of projectile fragmentation. It is confirmed by the general properties of the fragment energy spectra [7], shown in fig. 4. One observes that the maximum yield is close to the projectile velocity, and decreases slowly with decreasing ejectile mass. This can be accounted for by the fragmentation model.

Another example is provided by the data obtained for the $^{40}Ar + ^{69}Zn$ collision at 27.6 MeV per nucleon[8], presented in fig.5. The velocity v_F of the fragments $20 < A_F < 40$ normalized to that of the projectile v_p are shown as a function of the ejectile mass. One sees that for the heaviest fragments $v_F/v_p \sim 1$, as expected from a nucleon surface-exchange reaction. From P to Al, v_F/v_p decreases regularly to become roughly constant again for Mg, Na and Ne. One can make two kinds of estimate for the velocity of a fragment issuing from a fragmentation reaction : (i) If one assumes that, in the fragmentation process, the nucleons are removed from the projectile one after another and that an average of 8 MeV is required for each of them, then $v_F/v_p = [1 - 8(40 - A_F)/27.6\ A_F]^{\frac{1}{2}}$. This corresponds to the solid curve in fig. 5 (ii) If one

assumes that the projectile is sheared in two, then several bonds have to be broken simultaneously. The number of these bonds can be treated as proportional to the surface of contact between the two pieces of the projectile when starting from a spherical geometry. In this case, the velocity v_F of the outgoing fragments A_F may be expressed as :

$$v_F = v_p \cdot [1 - (2 E_s A_p / E_p A_F)]^{\frac{1}{2}}$$

where E_s is the separation energy.

In the abrasion picture, $E = 2 \gamma s$, where γ is the nuclear surface tension coefficient ($\sim$ 1 MeV/fm^2) and s the area of the surface between the abraded zone and the fragment (i.e. the intersection between a sphere and a cylinder). This expression yields the dotted curve. A satisfactory agreement is obtained with the data of fig. 5 for both calculations.

Again a strong indication for a fragmentation process is obtained from the correlation between the masses of the projectile-like and target-like fragment (fig. 6). The near proportionality observed is consistent with the abrasion model which correlates the mass losses of the two colliding nuclei.

An analysis in terms of fragmentation can be pushed further. In a purely geometrical picture, it can be assumed that the overlap region between target and projectile is sheared away to form a hot zone of nuclear matter, the "participants", whereas the remaining parts of the projectile and target, the "spectators", are only slightly perturbed. The abraded projectile almost preserves its initial direction and velocity, and carries a relatively small amount of excitation energy, which is proportional to the difference in surface energy between the deformed abraded nucleus and a spherical nucleus of the same volume. The excitation energy of the fragments is then dissipated by nucleon evaporation (ablation stage). Within this geometrical model, the mass distribution of the fragments is directly related to the impact parameter. The geometry problem of determining the intersecting volume of target and projectile nuclei as well as the area of the abraded fragments can be solved exactly by numerical integration techniques [16].

In fig. 7 a) the calculated mass distribution is compared to the experimental one for the reaction $^{40}Ar + {}^{27}Al$ using a radius parameter $r_o = 1.36$ fm. Also displayed in the figure is the calculated excitation energy of the primary fragments as a function of their mass. Considering the simplicity of the model, the agreement with the data in the intermediate mass region from ~ 17 to ~ 35, is surprisingly good. For fragments close to the projectile, the calculated yields are too large. Actually, one will see below that discrepancies occur almost systematicaly between the experimental results and fragmentation-model predictions for such fragments. It will be shown that they originate mostly from the dominance of direct transfer processes.

The lightest fragments, below mass 17, may be produced by various mechanisms and the disagreement between the calculations and the data does not necessarily imply a defect of the model. A more compelling evidence for the geometrical aspect of fragment production is given by fig. 7 b) where the calculated ratios of the mass yields between the $^{40}Ar + {}^{27}Al$ and $^{40}Ar + {}^{nat}Ti$ reactions are compared to the experimental ones. The mass dependence of this ratio is nicely reproduced and reflects essentially the difference in size between the Al and Ti target nuclei. They scale roughly as $A^{1/3}$.

Also the shape of the velocity spectra can be analysed in the framework of a clean-cut abrasion model according to the formalism of Goldhaber[9], as done for instance in ref[7]. In this model, the momentum distribution of a given fragment simply reflects the momentum distribution, assumed to be Gaussian-shaped, of nucleons inside the projectile. It is given by :

$$P(p) \propto \exp -[\,(p - p_o)^2/2\,\sigma^2\,]$$

where p_o is the momentum corresponding to the maximum of the distribution, while the dispersion about this value, σ, is given by :

$$\sigma = \sigma_o^2 A\,(A_p - A)/(A_p - 1)$$

and

$$\sigma_o = \langle p_F \rangle^2/3$$

where $\langle p_F \rangle^2$ is the mean square value of the single nucleon internal momentum

in the projectile, and where A and A_p stand for the masses of the ejectile and projectile, respectively.

A comparison between the experimental widths and the theoretical ones is given in fig.8. A satisfactory agreement with the above parabolic law is obtained for masses between 16 and 35 taking for σ_0 the value of 112 MeV/c directly derived from the electron scattering data. In the same figure are also drawn parabolas with σ_0 = 112 MeV/c ± 10 % in order to show the limits compatible with the data precision.

Below mass 16 or so the velocity spectra are so asymmetric and the low velocity tail becomes so important that it is no longer reasonable to compare the data with the Goldhaber picture.

1.2 Deviations from a clean-cut fragmentation model

Indeed the data of ref. [7] as displayed in fig.4 or, as contour plots, in fig. 9 show that the ejectile has a broad velocity spectrum extending far below the beam velocity. The shape of the contours in fig. 9 evolve rapidly with the size of the ejectile, for the asymmetry of the distribution as well as for the steepness of the peak. The lighter the ejectile, the more asymmetric the velocity distribution is. At such a small angle (3°), the spectra are quite representative of the longitudinal momentum dispersion. In addition to a major component essentially gaussian in shape, there is always a low velocity tail which grows with the decreasing ejectile mass. Such a behaviour is not reported at high bombarding energy [6].
Thus the data clearly exhibit some distorsions from what is expected in a simple fragmentation process.

This is confirmed by a systematic study of the variation of σ_0 with the mass of the ejectile. Fig. 10 taken from ref. [1] demonstrates the difference between the results observed at high (213 MeV per nucleon) [6] and at intermediate (27 MeV per nucleon) energy [8]. For the lower energy case, there are obviously two families of points. For masses below A_F = 35, the σ_0 value

is constant ($\sigma_0 \sim 84$ MeV/c) and close to the ones derived at 213 MeV per nucleon. But fragments close to the projectile have a much smaller reduced width close to 50 MeV/c. This apppears indicative of a direct surface transfer reaction. It will be analyzed in detail in the next section.

One more striking departure from the simple fragmentation model is found if one analyzes the transverse momentum distribution of the fragment. This is complementary to the study of the longitudinal distribution, derived (Fig. 4) from the velocity spectra of the fragments at very forward angle. The transverse momentum dispersions can be deduced from a fit to the fragment angular distributions or from contour plots such as those of fig. 9. Again the Goldhaber model[9] provides a parametrization of $\sigma_\perp$ in terms of σ_0, the variance of the momentum distribution of individual nucleons inside the nuclei, and of two more parameters, σ_β which arises from the deflection of the projectile in the field of the target, and σ_C which accounts for Coulomb scattering. Fig. 11 clearly shows that the model does not describe the data correctly.

Most authors, like in ref. [16], assign this discrepancy to the occurence of energy damping of the fragments, which cannot be reproduced in the framework of a simple statistical model.

Other limits to a description of the interaction as a fragmentation process can be seen in the analysis of the N/Z ratio of the fragments.

For instance the data collected in fig. 12 show the influence of the neutron excess of the target on the average neutron value of the fragment. When mean N/Z ratios of projectile-like fragments from the reaction 27 MeV/u Ar on ^{58}Ni, ^{64}Ni, ^{103}Rh and ^{197}Au are compared, strong odd-even effects are observed, whatever the target. Also a clear relationship appears between the N/Z of the target and N/Z of the ejectiles. The more n-rich the target is, the more n-rich the fragment is. This enrichment in neutrons is clearly due to the n-excess of the target and not to its size : ^{64}Ni and ^{103}Rh have the same N/Z ratio, 1.28, as compared to ^{58}Ni (1.07) and ^{197}Au(1.49).This

effect is in fact strongly enhanced when looking at the most n-rich products of a given element [10].

The influence of the target might be an indication that the interaction time, although very short ($< 10^{-22}$ sec), is still long enough to allow the exchange of a few nucleons between the two interacting nuclei. Another process might be the possible reabsorption of nucleons from the participant zone. Both effects are supposed to decrease with increasing energy. Larger effects are indeed observed, for the same system (Ar + Au), at 27 MeV than at 44 MeV per nucleon.

The above results are only a small part of the data which, over the last couple of years, have definitely documented the major feature of peripheral collisions at intermediate energy : they are dominated by a fragmentation process ; yet they exhibit deviations from that process which clearly show that mean-field effects, which are dominant at lower energies, are still at work.

This conclusion justifies that calculations be undertaken to account for the observed production cross section with simple geometrical models.

1.3 Calculation of fragmentation products at intermediate energy

Guerreau [12] calculates these cross sections using the simple abrasion ablation model. The mass distribution is calculated under purely geometrical considerations on the degree of overlap between the two interacting nuclei. Then the charge distribution is deduced assuming zero-point motion of the giant dipole resonance in the projectile [13]. Starting from the geometrical-model estimate for the excitation energy of the fragment, the deexcitation stage, which plays a major role for determining the eventual production of very unstable nuclei, is calculated using the code LILITA[14]. This deexcitation is calculated for all primary products (i.e. around 280 for an Ar induced reaction) and the final mass and charge distributions are deduced. Results of such a calculation are shown in fig.13 for the system 44 A.MeV Ar + Ta, and compared with experimental results obtained at GANIL on this system (closed circles) and those from a very similar system, 44 A.MeV Ar + Au [1] (open circles).

The agreement is quite satisfactory for the peaks of the distributions, with cross sections ranging between 1 and 100 mb, and still very good for the most neutron-rich isotopes observed. Thus this calculation has a valuable predictive ability which is used in the current search of very exotic nuclei at GANIL.

In another direction, Dayras and his coworkers[16] have developped an extended abrasion model to take into account in detail some kinematical effects of the collision. They note that even at relativistic energy, the velocities of the projectile fragments are slightly shifted downwards from the projectile velocity, indicating that the fragments have lost energy in the abrasion process. This slowing down of the projectile fragments has been successfully calculated, assuming that successive removal of bound nucleons from the projectile in the abrasion stage results in a frictional force. At intermediate energies, the energy damping of the fragments is more substantial, as illustrated in fig. 14 where the average kinetic energy per nucleon E_F/A of the fragments is plotted as a function of their mass. The energy loss increases almost linearly with the number of nucleons removed from the projectile. For fragments of a given mass, the energy loss tends to increase slightly and systematically with their charge number. In order to take into account this slowing down of the projectile-like fragments in the intermediate energy regime, an extension of the abrasion model, which includes kinematical effects, is proposed by Dayras et al[16].

Within this model, it is assumed that the energy damping of the fragments results essentially from the energy dissipated in order to split the projectile or (and) target into a spectator and a participant part.

Analytical expression can then be derived for all the kinematic observables under an explicit estimate of the energy released by the splitting of both the projectile and target into participant and spectator parts. In fact these separation energies are taken[16] as :

$$S = \alpha S_{abr} + (1 - \alpha) S_{gg}$$

where S_{gg} is the ground state separation energy calculated in the framework of the liquid drop model, and S_{abr} the separation energy as given by the geometrical abrasion model,

$$S_{abr} = 2 \gamma s,$$

where $\gamma \sim 0.95$ MeV/fm is the nuclear surface tension coefficient and s is the area of the interface between the abraded zone and the remaining fragment (see section II.1.1). A fraction of S given by α (S_{abr} - S_{gg}) will appear as excitation energy in the fragments and in the fireball. The factor α is a parameter which permits to vary the separation energies from their ground state value S_{gg} ($\alpha = 0$) to the value S_{abr} given by the abrasion model ($\alpha = 1$). It is expected to depend somewhat upon the interaction time (or relative energy between projectile and target). It should approach 1 at relativistic energies where fast clean-cut abrasion is expected. On the other hand, when the bombarding energy is decreased, the interaction time becomes sufficient to permit some rearrangement of the nucleons in the overlap region between projectile and target. This leads to a break-up configuration which is energetically more favourable corresponding to a value of α less than 1. In fact, in agreement with the above arguments, it was found [16] that using separation energies as given by clean-cut abrasion produces too large energy losses for the projectile fragments in both the $^{40}Ar + {}^{27}Al$ and $^{40}Ar + {}^{48}Ti$ reactions. Indeed values of α equal respectively to 0.4 and 0.8 give the best agreement with the data.

2. Transfer reactions

2.1 Experimental evidence

It was noted already that those fragments close to the projectile exhibited kinematical properties which were at variance with fragmentation (see fig 10). These results were attributed to the dominance of direct multi-nucleon transfer processes. A direct evidence for the occurence of such processes was obtained, as soon as GANIL operation started, when forward

emitted species with Z and/or N values larger than those of the projectile were observed (fig.15). Furthermore it appeared possible to account for the energy spectra of isotopes close to the projectile by DWBA calculations (fig.16).

A definite demonstration of the occurence of direct transfer process can be obtained through the result of a quasi exclusive experiment in which the fragments are observed in coincidence with light particles[19]. The latter are detected in a forward cone of 30°. Fig.17 strikingly demonstrates that most fragments close to the projectile emitted at forward angles (in the present case 4°) are not accompanied by the emission of a light particle. Even at such high energy (60 MeV per nucleon), pure transfer dominates, accounting for instance for 60 % of the cross section of Z = 17 fragments. It might be noted that for Z higher than the projectile value (Z = 18), the probability that a light particle is emitted in coincidence increases, indicating a more complex process which would associate transfer and subsequential deexcitation. Transfer probabilities appear to remain similar between 35 and 60 MeV per nucleon (fig.18) with little or no effect of the target.

For fragments which are further away from the projectile, the coincident emission of light particles is more probable (fig.17). Yet the influence of direct transfer is still apparent : it is shown[19] for instance that the (Z = 13) + α channel is dominated by sequential decay of a Z = 15 fragment with a rather well defined kinetic energy (fig.19).

2.2 The selectivity of transfer reactions at intermediate energy

Nucleon transfer between nuclei in the energy domain up to 20 MeV/u is well understood. It has been shown that spectroscopy of individual nuclear states is possible by use of heavy-ion transfer reactions. Specific dynamical properties of these reactions are connected to the "recoil effect" which leads to matching conditions as discussed e.g. by Brink[20]. At higher energies, nucleon transfer between low-lying states becomes smaller. It depends on the details of the momentum distributions since the center-of-mass momentum of the

transferred nucleon must be compatible with the momentum wave function of the initial and final states which have very little overlap at high relative velocity of the colliding nuclei. Fig. 20 gives a schematic representation of the two momentum distributions in a A + (b + c) → (A + c) + b transition.

Simple arguments based on energy and angular momentum conservation indicate that, in accordance with Brink's semi-classical matching rules[20] the transferred angular momentum must be large. A second rule which applies at high incident energy is illustrated in fig. 21, in the particular case of a $lp_{\frac{1}{2}}$, i. e. $j_<$, initial state of the transferred nucleus. From the fact (due to the relative high velocity of the projectile P and target T) that the angular momenta of the transferred nucleon in P and T point in opposite directions, it is shown that non spin flip is favoured. As a result, transitions $j_i = l_i \pm \frac{1}{2} \rightarrow j_f = l_f \pm \frac{1}{2}$ are favoured[22]. The results of a ^{208}Pb (^{16}O, ^{15}N) ^{209}Bi experiment provide striking confirmation of these rules (fig.22). Similar results were obtained for the one-neutron transfer (^{16}O, ^{15}O) transition, while angular distributions of the strongly populated states in the final nuclei were reproduced by DWBA calculations[22].

Since the selection rules are now clearly established, the way is open to the identification and study of states of very high spin resulting from the coupling of two (or three) holes or particles of high j by use of two-(or three-)particles transfer at high energy.

2.3 Identification of collective states at high excitation energies

The high angular momentum which can be transferred through the collision of two nuclei has been successfully used to form rotational states of very high spin, even with moderate incident energy[23].

The specific knowledge which appears to be gained by increasing the incident energy to a few tens of MeV per nucleon concerns giant resonances.

In the liquid-drop model, giant resonances are interpreted as collective vibrations of the nucleus. For example, the monopole resonance is a

compression mode whereas the other modes are associated with nuclear surface deformations. In electric isoscalar vibrations, all nucleons vibrate in phase. Conversely, in isovector modes, protons and neutrons vibrate out of phase, as do spin-up and spin-down nucleons in magnetic resonances.

Heavy ions are a very effective tool to excite giant resonances. Fig. 23 shows that the giant quadrupole resonance is strongly populated by the inelastic scattering of 44 MeV per nucleon ^{40}Ar projectiles. Moreover the differential cross sections are found to increase with incident energy [25] . For instance, fig. 24 exhibits the resonances observed by 200 MeV per nucleon C scattering on Au. These structures could correspond to the high-energy monophonon strength.

At intermediate energies, quasi-boson calculations predict that multiphonon excitations should be maximal. Fig. 25 presents some data for the ^{40}Ar+^{90}Zr reaction at 44 MeV per nucleon [24]. Bumps are visible up to 60 MeV excitation energy. At least three bumps are observed, at 50, 58 and 66 MeV, independently of angle.

In order to get a deeper understanding of these results a Fourier analysis has been performed. In order to eliminate the statistical fluctuations a filter is applied to the high frequencies of the Fourier transform spectrum and then the inverse Fourier transform is taken. In figure 26 the result of such an analysis is compared to the original spectrum. In the histogram which is the result of the analysis, the statistical fluctuations have been eliminated and only wide bumps are observed. This analysis allows a better definition of the positions of the structures. Figure 27 presents the same analysis performed on two spectra at different angles. This figure illustrates the fact that the structures appear at the same excitation energy, at least around the grazing angle [24]. However, whether those structures are independent of the incident energy but directly dependent of the target nucleus still is an open question due to conflicting results[24,27] . Theoretical studies [28] indicate that multiphonon excitations might be responsible for the population of these broad states.

III.- CENTRAL COLLISIONS AND EXCITED NUCLEAR SYSTEMS

1. Central collisions as a source of hot nuclei

A fundamental question open in nuclear physics concerns the maximum temperature at which a nucleus can be brought before it evaporates. It immediately appears that such words as "temperature" and "evaporate" cannot be used without caution. Is temperature the right concept to describe the properties of a nucleus of increasing internal energy ? How is the temperature to be defined for a limited and quantal object ? How to measure it ? Is "evaporate" the right concept to describe the phase transition which might occur with increasing internal energy ?

In the study of the more general problem of the equation of state, intermediate energy accelerators such as GANIL can participate in a very fruitful way, for the simple reason that higher temperature requires higher internal energy which can be reached only by higher incident energy in the collision.

Yet the experimental difficulties are overwhelming. Defining a target nucleus, a projectile and an incident energy does not define a precise thermodynamical state. Son one must select a restricted sub group of the possible nuclear systems. Such parameters as the multiplicity of light charged particles emitted are used to that purpose. It is precisely at this stage that one is confronted with what might be at present the most difficult contradiction of this study. On one hand, one must carefully identify the actual individual processes, which imposes extremely exclusive experiments, but at the risk of making detailed studies of microscopic aspects of the whole

And indeed, even if rather precise thermodynamical conditions are experimentally defined for the system formed in the collision, it remains difficult to formulate and measure a "temperature" from experimental results, because of at least two major problems. First, one must ascertain that the composite system is truly isothermic, i.e. that the temperature is the same in all parts of the nuclear system at a given time. Second, heat dissipation, which occurs through the evaporation of particles of fragments, reduces the internal excitation energy of the system, hence implies a variation of the temperature with time. Experiments try to overcome these problems. From the above discussion, it is clear that the choice of experimental filters to identify the process is essential. It is illustrated in the cases described below.

2. Disappearance of fusion with increasing incident energy

The bombardment of a heavy nucleus like Uranium by a projectile like e.g. ^{40}Ar can lead to fission products in two ways. In case of a peripheral collision, the recoiling U- like nucleus is excited and undergoes fission. In case of a central collision, which is expected to lead to complete or partial fusion, the compound nucleus also fissions. In the first case, the recoil velocity of the fissioning nucleus is low, while in the second case it represents a large fraction of the center-of-mass velocity. This difference is kinematically reflected in the angular correlation between the fission fragments. Thus, the two processes can be distinguished by measuring the angle between the directions of these fragments : the smaller the correlation angle, the higher the velocity of the recoiling fissioning nucleus, i.e. the higher the momentum transfer (fig. 28). This powerful and very illustrative method has given strikingly clear results (fig. 29). They confirm in more details and in a quantitative way what could be anticipated from the result shown in fig. 2 : the fusion-fission process disappears rather abruptly around 40 MeV per nucleon for the Ar + Th system.

Similar evidence is obtained from a study [31] of the $^{40}Ar + {}^{27}Al$ system. The experimental advantage of reverse kinematics, i.e. that all the products of the reaction can be detected in a narrow forward cone in the laboratory, is put to use to observe the products of both direct and damped reactions (fig.30). The damped component disappears progressively when the energy is raised from 27 to 40 MeV per nucleon.

A quantitative measure of this disappearance is obtained [31] from a comparison of each energy spectrum for a given E_{inc} with the corresponding spectrum at E_{inc} = 40 MeV per nucleon through the measurement of chi-square (χ^2) defined as

$$\chi^2 = 1/N \left[\sum_{j=1}^{N} (b_j - a_j)\,(b_j - a_j) \right]^{-1/2}$$

where a_j (respectively b_j) are the amplitudes for the channel j at the considered energy (respectively 40 MeV/amu), and N the normalisation factor equal to the number of channels on which the χ^2 is calculated. Fig. 31 shows the χ^2 values for various residues as a function of the beam energy per nucleon. It can be clearly seen that, whereas the 36 and 40 MeV/amu data do not exhibit susbtantial variations, the lowest energy data (27 MeV/amu) differ in a large extent because of the amount of the evaporation residue component.

The net result is that the evaporation residue component vanishes for beam energies in excess of 32-36 MeV per nucleon, which is close to the value which would be derived from fig. 29 in the very different case of the Ar + Th system. It is also interesting to relate this result to other observations concerning the drastic reduction of the cross section for fusion-like products at 44 MeV per nucleon in the collision of Ar with a variety of targets, as discussed by Borderie and Rivet [32]. One would then suggest that the relative velocity is the parameter which governs the disappearance of fusion-like reactions. Yet several results obtained with a ^{12}C beam indicate that quasi-fusion processes are still effective at considerably higher energies [33,34].

It might then be more realistic to assign the disappearance of fusion with increasing energy to a threshold effect due to a limitation in the excitation energy that a nucleus can sustain. This effect, predicted by Bonche and coworkers [35], would lead for instance to a maximum temperature of 7.5 MeV at A = 60 (Ref. [36]). This is close to the experimental result indicated above for ref. 29. The limiting temperature is also predicted to decrease with increasing mass of the composite nucleus, in qualitative agreement with experimental results.

3. Measuring the temperature of excited nuclear systems

As indicated above, the thermodynamical state of the nuclear system formed in a collision is by far not unique. It depends upon the impact parameter and it varies as time elapses, in the same way as a classical system would. Furthermore, it is subjected to all the variations expected for a quantum system, already in the entrance channel, and more and more so as the collision develops among the quantal channels open to the system. Thus the extraction from an experimental result of the temperature of a system is an arduous task which must be restricted by at least a crude estimate of parameters such as the impact parameter, or the total angular momentum, or the linear momentum transferred to the system, or the stage of the reaction process at which the temperature is measured, etc...

The success of the semi-classical description [37] based on the Landau-Vlasov equation allows to illustrate the above points. Fig. 32 shows in particular that the system is not thermalized until some 80 fm.c^{-1}, or about 3×10^{-21} s, since, before that time, the momentum distribution of nucleons is

In this case, their energy might truly inform us on the temperature value.

3.1 Temperature from the energy spectrum of particles

Indeed the shape of the kinetic energy spectra of light particles emitted in the collision of two nuclei can be related to the temperature of the emitting source by the statistical theory [39,40]. The energy spectrum of a particle is expressed as

$$W(E)\,dE = [(E - E_{thresh})/T2] \exp [-(E-E_{thresh}/T)]\,dE$$

where E_{thresh} is the threshold energy for the emission of the particle, i.e the corresponding coulomb barrier. The main advantage of the method is that it is free of any assumption about nuclear state densities. But of course the above formula holds only as long as the particles are emitted by one given nuclear species at a specific temperature. The method can thus be fruitful or erroneous depending on the cases in which it is applied. At high incident energy, the smooth decrease with E given by that formula might reasonably reproduce the data, yet unrealistic values of T might be extracted from such a fit. In the case of 44 MeV/uma Ar projectiles on Au, a temperature as high as 15 MeV is deduced. It is certainly grossly overestimated since, under the assumption of a Fermi gaz where the excitation energy E* is equal to aT^2, with the level density parameter a taken usually as A/8 in MeV^{-1}, a 15 MeV temperature corresponds to an excitation energy of some 30 MeV per nucleon. It considerably exceeds the well known binding energy of about 8 MeV per nucleon. Obviously no nuclear isothermic source can exist with such a temperature. This illustrates the necessity of more exclusive experiments since inclusive spectra do not distinguish between the different contributing mechanisms. In particular, since these particles can be emitted not by primary fragments, but by those which have already undergone emissions of various kinds, the energy spectrum is accordingly broadened in a way that, as statistical calculations have shown, can increase the apparent temperature by a factor of 2.

A more realistic value of the temperature can be obtained from more exclusive experiments under reasonable assumptions for the reaction process. If one assumes that after a Ar + U collision, some of the particles are emitted from a thermalized, hot and deformed rotating system, and the other by fully accelerated but rather cold fragments, a good fit to the data can be obtained with a 8 MeV temperature for the composite system (fig. 33).

Thus, while the extraction of temperature from inclusive data is quite unreliable, useful results can be reached from the energy spectra of the light particles emitted in the reaction if the emitting nucleus is detected in coincidence with the evaporated particles, and if the consistency of the results is checked by varying the detection angles, in particular to test that the emission is isotopic, a good proof that thermalization has been achieved.

3.2 Temperature from the ratio of populations of different states

If a nuclear fragment is emitted from a thermalized nucleus, the various possible quantum states of the fragment, characterized by their excitation energy E*, should appear with a probability P which decreases exponentially with E* according to the Maxwell-Boltzmann statistics. More precisely, P will be proportional to exp (-E*/T). Thus the population ratio between two states of energy E^*_1 and E^*_2 will be $R = \exp [-(E^*_1-E^*_2)/T]$.

The two states might be particle stable, in which case they might be detected directly or through their decay γ rays (see e.g. ref. [41]). If the clusters are particle unstable, the fragments from their desintegration might be detected in coincidence (see, e.g., ref. [42]). An example of the results obtained by this method is given in fig. 34.

It shows the coincidence yield for the two products resulting from the decay of a Li cluster versus their relative kinetic energy. One observes two bumps corresponding to two excited states of the cluster. Their relative abundance may be used to determine a temperature. Are these temperature values reliable ? The method may be correct only if the observed clusters simply

reflect the thermal state of the source, i.e. if the observed decay by cluster emission is a primary one. "Side feeding" produced by previous decay branches would obviously distort the simple relationship between the ratio R and the temperature T indicated above, resulting in an erroneous estimate of the temperature. Although the side feeding effect can be calculated [43,44], some caution must be used when drawing conclusions from limited data, and ref. [40] contains a thorough analysis of the experimental and theoretical problems involved. Yet the comparaison between several cluster channels [44] and the observed consistency between the extracted temperature values points to the validity of the method. An example is given in fig. 35 and 36.

3.3 Other methods and conclusions

In a recent review [40] , Tamain has outlined that other experimental parameters shed light on the properties of thermalized nuclear systems, hence on their temperature. In particular any way to measure the excitation energy of a hot composite system might lead to an estimate of the temperature.

One such way consists in the measurement of the multiplicity of the evaporated particles. For instance it was shown [46] that the number of emitted neutrons is correlated with the folding angle of the fission fragments into which the compound system ultimately decays (fig. 37). The latter one being correlated itself with the momentum transfer and the impact parameter, as discussed in section III2, a consistent overall picture emerges. The average energy carried away by each neutron can be estimated, although with one drawback, namely that this procedure is obviously model-dependent. This results in the knowledge of the total excitation energy E* of the composite system.

Another estimate comes from the recoil velocity of the composite system. The kinetic energy lost in the collision might be assigned to internal excitation energy. Again, the value of E* is transferred into a temperature value by assuming that the hot composite system is a Fermi gaz for which

$E^* = a\,T^2$ where a is the level-density parameter, as discussed already in section III 3.1.

One sees that temperature measurements are difficult. The relevance of the concept, as discussed above, must be seriously ascertained and its use properly restricted. In spite of the difficulties, both theoretical and experimental, it is now established that hot thermalized systems have been formed and observed with temperatures of at least 5 MeV. Wether higher temperatures can be reached, possibly in excess of the nuclear binding energy, which specific decay modes would occur for such states, these are some of the open and puzzling questions.

4. Developments

4.1 *Detailed study of limited hot systems*

As the collision between two nuclei develops, partial thermalization might occur for a limited and well separated set of nucleons. Careful coincidence measurements are of utmost importance since the nuclear system as a whole, as it results from the collision, is highly unhomogeneous[47].

In particular, an analysis of the momentum correlation of two light particles emitted simultaneously in ^{40}Ar-induced reactions on ^{197}Au at 60 MeV per nucleon has been performed[48]. It is expected to provide an estimate of the size of the emitting source according to the classical Hanburry-Brown and Twiss procedure [49].

The main result already obtained is illustrated by fig. 38. There is an unmistakable variation in the spacetime localization of the emission of coincident particles. Namely, the emitting subsystem grows larger as the impact parameter decreases, and the number of violently interacting nucleons increases.

4.2. Calculating the dynamics of the collision.

The detailed calculation of how the whole set of nucleons reacts and evolves with time in the collision of two nuclei at intermediate energy is a serious challenge. Yet it is a clear necessity if one is to extract, from the simple phenomenological description of observed parameters, a physical image of broader significance. What makes such a calculation a challenge around the Fermi energy is that none of the simplifications used at lower and higher energies are legitimate. At intermediate energy the deposition of energy into the nuclear system results from a dynamical balance between one - and two - body dissipation.

Solving the nuclear Landau-Vlasov equation has proven to be both possible and effective [37,50]. The diffuseness of the nuclear surface, the long-range effects of the Coulomb interaction, the short range nuclear field and the residual interaction must be and have been included. Thus, a reliable model is now available to analyze the experimental results and search for the specific nuclear properties at the limit when the excitation energy deposited into the nuclear system can lead to its disassembly. The lecture by C. Grégoire at this school describes this important development.

4.3. The onset of multifragmentation

The disappearance of fusion with increasing incident energy is now well documented, as discussed in section III, 2. It appears that the maximum excitation energy or temperature that a nuclear system can sustain has been reached. The way in which a nucleus reacts when this limit is trespassed would certainly be very informative on the properties of nuclear systems.

There is no doubt that the disassembly of the system results into the emission of nuclear fragments. Nuclear chemists, long ago, have collected an impressive and consistent amount of evidence which shows that the probability of the fragment emission decreases with Z (but is still sizable for Z larger than 10), when a heavy nucleus is hit by a light particle of some hundreds of

MeV or a few GeV of energy. Now, the detailed study of nucleus-nucleus collisions around 30-50 MeV per nucleon allows to address the following question : does the highly excited nuclear system decay into all the many channels open to fragmentation in a purely statistical manner ? Or does the excited N-body quantal system break up into a few large pieces in a non-linear, non-statistical way ? In other words, are there structural instabilities which prevent the heated system to evolve as a gaz-like system would ? Multi-fragmentation is suspected to occur, but no definite evidence is yet obtained. It is expected that exclusive experiments will allow to observe and, if the theoretical models which predict its occurence are right, to study this novel phenomenon in the next few years.

IV. - SYNTHESIS OF NEW NUCLEAR SPECIES IN INTERMEDIATE ENERGY HEAVY-ION COLLISIONS

The importance of fragmentation-like processes at intermediate energy has opened a new and very efficient way to produce nuclei far from stability. Its effectiveness was first demonstrated at higher energies, around one GeV per nucleon, since such beams were available first. The Z and N distributions of the projectile fragments being governed by statistics, they contain sizable yields of unusual Z, N combinations. Pionneering work along this line was done at the BEVALAC in 1979[51].

The availability of new heavy-ion accelerators, with energies reaching 100 MeV per nucleon, but intensities much higher than those obtainable at the BEVALAC or SATURNE, opens a possibility to dramatically extend the usefulness of that method.

Fragmentation at, say, 50 MeV per nucleon is certainly not the clear process observed at much higher energy, as discussed in chapter I. Indeed, two important factors are lost by decreasing the energy. First, effective targets are simply thinner, by up to two orders of magnitude. Second, the momentum distribution of the fragments, which in first order results from the inner

momenta of participant nucleons within the projectile (see section I), is relatively broader at GANIL than at BEVALAC energies, hence the collection of fragments is less efficient, by about one order of magnitude. Yet the fact that the intensities available at GANIL for the projectiles of interest reach 5 x 10 pps and are expected to increase over the years offers an unmatched opportunity to produce new exotic isotopes.

1. Towards the proton and neutron drip lines

Knowing that an isotope is bound or not for proton or neutron emission puts a limit on its binding energy, and allows a comparison with the large number of theoretical mass predictions[52]. The fragmentation-like process of projectiles at GANIL has been used to push the limits of experimentally observed nuclei further toward the drip line.

The prime requirement of such investigations is to detect and identify fast projectile fragments with as high an efficiency and as low a background as possible. A double magnetic system called LISE [53] was built to best meet this requirement. Fragments selected according to their A/Z values are collected in a low-background room by a triple-focusing system within the 5 % momentum acceptance of the magnetic system. Further fragment selection, accomplished by using an energy degrader between the two dipoles, has been successfully realized[54].

This last improvement has proven to be of utmost importance. It dramatically restricts the number of collected nuclear species from a few tens (see fig. 39) to three or four only (see fig. 40). It has probably done, at a very low cost, more than a gain of a factor of 10 in incident energy would have accomplished. Indeed, at GANIL energies, for the parameters mentionned, the limiting factor is the counting rate in the telescope located at the focal point of LISE. Getting rid of most of the abundant species has allowed to make full use of the momentum aperture of the magnet and of the beam intensity. To give only one example, the collection rate of the exotic ^{31}Ar isotope has gone

from 3 X 10^{-3} to 1 per second by using the extra selection provided by the energy degrader.

In successive runs over the last two years, many isotopes were observed. From an ^{44}Ar projectile, ^{23}N, ^{29}Ne, ^{30}Ne (ref.[15]) and even ^{22}C (ref.[55]) were observed, while the unbound character of ^{21}C and ^{25}O was established. The fragmentation of neutron rich ^{86}Kr projectiles yielded fourteen new isotopes [56].

On the neutron-rich side, the neutron drip line appears to be reached all the way up to Z = 7. The relevance of the type of results reported here is well illustrated by the case of ^{29}Ne that all mass predictions but one[57] found unbound and which was definitely observed [15]. It might be relevant to note that with Z = 10 and N = 19, this isotope, for which a binding energy larger than predicted by systematics or extrapolations is observed, lies very close to the Z = 11-12, N = 20 nuclei. This is an area of very strong deformation [58] at the expected location of a closed shell. That case indeed has provided a clear example of the unique and fundamental information on nuclear models that the study of exotic nuclei can contribute.

On the proton-rich size, the use of ^{40}Ca projectiles allowed the observation of Tz = - 5/2 isotopes, ^{23}Si, ^{27}S, ^{31}Ar and ^{35}Ca (ref.[59]) and even ^{22}Si (ref.[60] (fig.40)]. From a run with a ^{58}Ni beam, twelve new isotopes could be reported (ref. [61] (fig. 39).

As a result of the observation of ^{22}Si, the proton drip- line is now reached up to Z = 20.

2. Some properties of exotic nuclei

Although the mere observation of new isotopes carries useful information, as examplified above, and because it puts any theoretical estimate of nuclear binding energies to a test, exotic nuclei have more to offer. May be simply in helping to understand what we mean by the existence of a nucleus and in extending the concept of radioactivity (fig. 41).

As an illustration let us discuss the prospects for observing some new radioactive processes.

2.1. The search for new radioactive modes.

The concept of radioactivity has greatly benefited in the last few years of the discovery of new radioactive processes. Some new ones might be obtainable through the improved production of exotic nuclei provided by intermediate-energy heavy-ion beams.

A very fascinating process would be two-proton radioactivity. Pairing energy effects make the binding energy of many even-Z proton-rich nuclei stronger against one-proton than two-protons emission. At the proton drip line, it might happen that a nucleus is thus bound for one proton emission but is able to decay by the emission of two protons. This process was discussed long ago by Goldansky [62] and Jänecke [63]. The probability of this emission is governed by barrier penetration which itself strongly depends upon the kinematics of the two protons. It is generally predicted that the configuration most likely to speed up the crossing of the barrier corresponds to two correlated protons equally sharing the available energy.

Some light nuclei which can be produced from GANIL projectiles are good candidates to exhibit 2p radioactivity. Their negative binding energy (E_{2p}) should not lie below about - 0.8 or - 1 MeV so that the $T_{\frac{1}{2}}$ (2p) value is not so short as to make the nucleus decay before it is detected. And it should not lie above about - 0.3 or - 0.4 MeV so that the $T_{\frac{1}{2}}$ (2p) value is not so much longer than the competing $T_{\frac{1}{2}}$ (β) value as to make the 2p branching ratio vanishingly small. Thus a narrow energy window, say - 0.4 > E_{2p} > - 0.8 MeV, exists for potential candidates to 2p radioactivity with Z values around 15 or 20.

The nucleus ^{31}Ar, which can be produced at a rate of about one per second at GANIL, appeared to be a possible candidate for 2p radioactivity since the predicted E_{2p} value, of the order of 200 keV, was, within typical

uncertainties, close to the above energy window. Yet it is found that the half life of ^{31}Ar, 15 ± 3 ms[64], is not reduced from the expected ß-decay half life, hence that the 2p process, if present, is quite marginal.

Another candidate is ^{39}Ti with a predicted E_{2p} value of about 700 keV. It is still to be observed (see fig. 39), but lies now within reach of GANIL experiments.

Candidates for neutron radioactivity were proposed long ago as long lived isomers with very high spin, among neutron-rich nuclei of the fp shell[65]. The neutron radioactivity process depends drastically upon the difference between the energy locations of such a high-spin configuration and the neutron emission threshold. Thus precise predictions are particulary difficult. Yet such situations are probably bound to occur. This makes the search for neutron radioactivity legitimate, even if difficult, especially since, some of the candidates identified, such as ^{67}Fe, can be obtained at GANIL. It should be remembered that proton radioactivity was first observed from an isomeric state [66, 67].

2.2. Binding energies

The knowledge of the binding energy of a nucleus provides a stringent test of nuclear forces, especially in the case of exotic nuclei which have an unusual unbalance of protons and neutrons. Indeed predictions widely differ between themselves far from stability and, even with limited accuracy, experimental results are quite discriminatory and enlightening. The variation of the binding energy along a series of isotopes also reveals fundamental nuclear properties such as shell closure effects or onsets of deformation [68,69].

Thus the fact that new isotopes are produced at GANIL with large yields opens the possibility of a broad investigation of binding energies of light nuclei far from stability. The absolute measurement of the nuclear mass must be accomplished with an uncertainty much smaller than 1 MeV to provide useful

information. For a nucleus of interest, all the collected events must then be free of spurious background counts, and the relative FWHM of the two parameters necessary to identify the isotope must be at most a few 10^{-4}. The accuracy on the peak centroid, a portion of the FWHM which decreases with increasing statistics, can then reach the required level of a few 10^{-5}.

A very powerful method to reach that goal has been developped at GANIL. The nature and energy of a fragment produced are extracted from two parameters known with a remarkably high accuracy. Its magnetic rigidity is measured by the SPEG spectrometer with a FWHM of 10^{-4}. Its time of flight is determined along a flight path some 100 meters long, since the target is exceptionally located near the exit of the second and last sector-separated cyclotron of GANIL, while the fragment is detected in the focal plane of SPEG. New mass values with accuracy better than 500 keV (fig. 42) have already been reported [70] for $^{20-21}$N, ^{23}O, $^{24-25-26}$F and new data are being analyzed. They are expected to give improved results, with uncertainties around 200 keV, for some 12 new isotopes. They will bring new information on the behaviour of neutron-rich nuclei near N = 20, where the very strong deformation observed at Z = 11 (as mentionned in § IV.1) seems to quickly disappear for increasing values of Z [72].

There lies clearly a concrete possibility of obtaining systematically the binding energy surface of light nuclei, which should stimulate theoretical efforts in this field.

V FINAL REMARKS

The study of nucleus-nucleus collisions at intermediate energy has been vigorously undertaken under the intuitive assumption that, when the relative velocity crosses the Fermi velocity of nucleons, the nuclear system would undergo a change from meanfield behaviour to one governed by the existence of individual nucleons. And physicists have learned by experience, over and over, that such transitions are prone to exhibit new and enlightening properties.

So far the experimental results have brought a general description of the observed phenomena. This lecture has attempted to describe most of the open questions, but not all. Among the missing one, the mechanism by which sub-threshold pions or hard protons are emitted is of great potential interest, since it probes possible cooperative processes, or the onset of the propagation of the collision in the nuclear medium.

Wether the great potential richness of all these studies rapidly gives ripe fruits is still an open question. One can imagine a rather pessimistic script for the forthcoming years of intermediate energy heavy-ion physics. Experiments would go more and more exclusive, and at the same rate the understanding of the phenomena would go more and more complex, technical, a hopeless average of low - and high - energy behaviours with no new vista on the properties of the excited nuclear system. One would be left with better tools for treating the difficult problem of many interacting fermions, and a crop of new beautiful results such as those presented in section IV for new nuclear species,but no new real insight into the properties of nuclear matter. A more optimistic future would lead us, after the necessary phase of accumulation of experimental facts and development of appropriate tools of analysis, to a broader and more general theory of the structure and dynamics of that specific object - A fermions in strong interaction - that nuclear physics examines.

REFERENCES

(1) D. GUERREAU : Nucl. Phys., A447, 37c (1985).

(2) C. GREGOIRE and F. SCHEUTER : Phys. Lett., 146B, 21 (1984).

(3) J.P. BLAIZOT : Phys. Reports, 64, 171 (1980)

(4) J. BLACHOT, J. CRANCON, B. de GONCOURT, A. GIZON, A. LLERES and H. NIFENECKER, XXIII Inter. Winter Meeting (Bormio, 1985) p. 598.

(5) D. GUERREAU, V. BORREL, J. JACQUET, J. GALIN, B. GATTY and X. TARRAGO : Phys. Lett., 131B, 293 (1983).

(6) Y.P. VIYOGI, J.M. SYMONS, P. DOLL, D.E. GREINER, H.H. HECKMAN, D.L. HENDRIE, P.J. LINDSTROM, J. MAHONEY, D.K. SCOTT, K. van BIBBER, G.D. WESTFALL, H. WIEMAN, H.J. CRAWFORD, C. Mc PARLAND, C.K. GELBKE : Phys. Rev. Lett. 42, 33 (1979).

(7) V. BORREL, D. GUERREAU, J. GALIN, B. GATTY, D. JACQUET, X. TARRAGO : Phys. A, 314, 191 (1983).

(8) F. RAMI, J.P. COFFIN, G. GUILLAUME, B. HEUSCH, P. WAGNER, A. FAHLI and P. FINTZ : Nuclear Physics, A444, 325 (1985).

(9) A.S. GOLDHABER : Phys. Lett., 53B, 306 (1974).

(10) V. BORREL, B. GATTY, D. JACQUET, D. GUERREAU and J. GALIN : Z. Phys. A324, 205 (1986).

(11) R. CONIGLIONE, G. LANZANO, A. PAGANO, J. BARRETTE, B. BERTHIER, D.M. DE CASTRO RIZZO, O. CISSE, R. DAYRAS, R. LEGRAIN, M.C. MERMAZ, H. DELAGRANGE, W. MITTIG and B. HEUSCH : Nucl. Phys., A447, 95c (1985).

(12) D. GUERREAU : proc. of HICOFEO Conf. (Caen 1986), J. de Phys., C4, 207 (1986).

(13) D.J. MORRISSEY, W.R. MARSH, O. JOTTO, W. LOVELAND and G.T. SEABORG : Phys. Rev., C18, 1267 (1978).

(14) LILITA, a Monte-Carlo Hauser-Feshbach code, J. GOMEZ del CAMPO and R.G. STOKSTAD : ORNL - TM - 7295 (Oak-Ridge Nat. Lab.).

(15) M. LANGEVIN, E. QUINIOU, M. BERNAS, J. GALIN, J.C. JACMART, F. NAULIN, F. POUGHEON, R. ANNE, C. DETRAZ, D. GUERREAU, D. GUILLEMAUD-MUELLER and A.C. MUELLER : Phys. Lett., 150B, 71 (1985).

(16) R. DAYRAS, A. PAGANO, J. BARRETTE, B. BERTHIER, D.M. DE CASTRO RIZZO, E. CHAVEZ, O. CISSE, R. LEGRAIN, M.C. MERMAZ, E.C. POLLACO, H. DELAGRANGE, W. MITTIG, B. HEUSCH, R. CONIGLIONE, G. LANZANO and A. PALMERI : Nuclear Physics, A460, 299 (1986).

(17) J. BARRETTE, B. BERTHIER, E. CHAVEZ, R. DAYRAS, R. LEGRAIN, M.C. MERMAZ, A. PAGANO, E. POLLACO, H. DELAGRANGE, W. MITTIG, B. HEUSCH, G. LANZANO and A. PALMERI : proc. of XXII Int. Winter Meeting (Bormio, 1984), p. 561.

(18) M.C. MERMAZ, V. BORREL, J. GALIN, B. GATTY, D. JACQUET and D. GUERREAU : Z. Phys. A324, 217 (1986).

(19) G. BIZARD, R. BROU, H. DOUBRE, A. DROUET, F. GUILBAULT, F. HANAPPE, J.M. HARASSE, J.L. LAVILLE, C. LEBRUN, A. OUBAHADOU, J.P. PATRY, J. PETER, G. PLOYART, J.C. STECKMEYER and B. TAMAIN, Phys. Lett. B172, 301 (1986) ; and communication to Bormio Winter Meeting (1987).

(20) D.M. BRINK : Phys. Lett. 40B, 37 (1972).

(21) W. von OERTZEN : Phys. Lett., 151B, 95 (1985).

(22) J. BARRETTE, B. BERTHIER, J. GASTEBOIS, A. GILLIBERT, R. LUCAS, J. MATUSZEK, M.C. MERMAZ, A. MICZAIKA, E. van RENTERGHEM, T. SUOMIJÄRVI, A. BOUCENA, D. DISDIER, L. KRAUS, I. LINCK, B. LOTT, V. RAUCH, E. REIBMESTER, F. SCHEIBLING, J.C. SENS, N. SCHULZ, C. GRUNBERG, W. MITTIG : proc. of HICOFED Conf. (Caen 1986), J. de Phys., C4, 179 (1986).

(23) J. SHARPEY-SCHAFER : Nucl. Phys., A447, 233c (1985).

(24) N. FRASCARIA, Y. BLUMENFELD, Ph. CHOMAZ, J.P. GARRON, J.C. JACMART, J.C. ROYNETTE and T. SUOMIJARVI : Nucl. Phys. (1987), in print.

(25) P. CHOMAZ : proc. HICOFED Conf. (Caen 1986), J. de Phys. C4, 155 (1986).

(26) J. ARVIEUX, B. BONIN, G. BRUGE, M. BUENERD, C. CERRUTI, J. CHAUVIN, J.Y. HOSTACHY; D. LEBRUN, J.C. LUGOL, L. PAPINEAU, P. ROUSSEL : Proc. Int. Nucl. Phys. Conf. (Harrogate 1986), Vol. 1, p. 82.

(27) S. FORTIER, S. GALES, C. OJALALI, S. AUSTIN, W. BENENSON, G. CRAWLEY, H. VAN DER PFLICHT and J. WINFIELD, to be published.

(28) P. CHOMAZ, NGUYEN VAN GIAI and D. VAUTHERIN : Preprint Orsay (1986), IPNO-TH 86-32, and to be published.

(29) S. LERAY : proc. HICOFED Conf. (Caen 1986), p. 275.

(30) M. CONJEAUD, S. HARAR, M. MOSTEFAI, E.C. POLLACO, C. VOLANT, Y. CASSAGNOU, R. DAYRAS, R. LEGRAIN, H. OESCHLER and F. SAINT-LAURENT : Phys. Lett., 159B, 244 (1985).

(31) G. AUGER, E. PLAGNOL, D. JOUAN; C. GUET, D. HEUER, M. MAUREL, N. NIFENECKER, C. RISTORI, F. SCHUSSLER, H. DOUBRE and C. GREGOIRE : Phys. Lett., 169B, 161 (1986).

(32) B. BORDERIE and M.F. RIVET : Z. Phys. A321, 703 (1985).

(33) D. HEUER, R. BERTHOLET, C. GUET, M. MAUREL, H. NIFENECKER, Ch. RISTORI and F. SCHUSSLER : Phys. Lett., 161B, 269 (1985).

(34) W. MITTIG, A. CUNSOLO, A. FOTI, J.P. WIELECZKO, F. AUGER, B. BERTHIER, J.M. PASCAUD, J. QUEBERT, E. PLAGNOL : Phys. Lett., 154B, 259 (1985).

(35) P. BONCHE, S. LEVIT and D. VAUTHERIN : Nucl. Phys., A436, 265 (1985).

(36) S. LEVIT and P. BONCHE : Nucl. Phys., A437, 426 (1985).

(37) C. GREGOIRE, B. REMAUD, F. SCHEUTER and F. SEBILLE : Nucl. Phys., A436, 365 (1985).

(41) D.J. MORRISSEY, W. BENENSON, E. KASHY, C. BLOCH, M. LOWE, R.A. BLUE, R.M. RONNINGEN, B. SHERRILL and H. UTSUNOMIYA : Phys. Rev., C32, 877 (1985).

(42) J. POCHODZALLA, W.A. FRIEDMAN, C.K. GELBKE, W.G. LYNCH, M. MAIER, O. ARDOUIN, H. DELAGRANGE, H. DOUBRE, C. GREGOIRE, A. KYANOWSKI, W. MITTIG, A. PEGHAIRE, J. PETER, F. SAINT-LAURENT, Y.P. VIYOGI, B. ZWIEGLINSKI, G. BIZARD, F. LEFEBVRES, B. TAMAIN and J. QUEBERT : Phys. Rev. Lett., 55, 177 (1985) and Phys. Lett., 1618, 275 (1985).

(43) H.M. XU, D.J. FIELDS, W.G. LYNCH, M.B. TSANG, C.K. GELBKE, D. HAHN, M.R. MAIER, D.J. MORRISSEY, J. POCHODZALLA, H. STOCKER, D.G. SARANTITES, L.G. SOBOTKA, M.L. HALBERT and D.G. HENSLEY : Phys. Lett., 1828, 155 (1986).

(44) D. HAHN and H. STÖCKER : Phys. Rev., C35, 1311 (1987).

(45) J. POCHODZALLA, W.A. FRIEDMAN, C.K. GELBKE, W.G. LYNCH, M. MAIER, O. ARDOUIN, H. DELAGRANGE, H. DOUBRE, C. GREGOIRE, A. KYANOWSKI, W. MITTIG, A. PEGHAIRE, J. PETER, F. SAINT-LAURENT, Y.P. VIYOGI, B. ZWIEGLINSKI, G. BIZARD, F. LEFEBVRES, B. TAMAIN and J. QUEBERT : Phys. Lett., 1618, 275 (1985).

(46) J. GALIN : Nucl. Phys., A447, 519c (1986).

(47) G. RUDOLF, J.C. ADLOFF, A. KAMILI, F. SCHEIBLING, B. BOISHU, A. GENOUX-LUBAIN, C. LE BRUN, J.F. LECOLLEY, F. LEFEBVRES, M. LOUVEL, R. REGIMBART, O. GRANIER, S. LERAY, R. LUCAS, C. MAZUR, C. NGO, M. RIBRAG and E. TOMASI : Phys. Rev. Lett., 57, 2905 (1986).

(48) A. KYANOWSKI, F. SAINT-LAURENT, O. ARDOUIN, H. DELAGRANGE, H. DOUBRE, C. GREGOIRE, W. MITTIG, A. PEGHAIRE, J. PETER, Y.P. VIYOGI, B. ZWIEGLINSKI, J. QUEBERT, G. BIZARD, F. LEFEBVRES, B. TAMAIN, J. POCHODZALLA, C.K. GELBKE, W. LYNCH and M. MAIER : Phys. Lett., 8181, 43 (1986).

(49) R. HANBURRY-BROWN and R.Q. TWISS : Nature, 177, 27 (1956).

(50) B. REMAUD, C. GREGOIRE, F. SEBILLE and L. VINET : Phys. Lett., 180, 198 (1986) ; C. GREGOIRE, B. REMAUD, F. SEBILLE, L. VINET and Y. RAFFRAY : Nucl. Phys., A465, 317 (1986).

(51) T.J.M. SYMONS, Y.P. VIYOGI, G.D. WESTFALL, P. DOLL, D.E. GREINER, H. FARAGGI, P.J. LINDSTROM, D.K. SCOTT, H.J. CRAWFORD and C. McPARLAND : Phys. Rev. Lett., 42, 40 (1979).

(52) S. MARIPUU ed. : At. Data and Nucl. Data Tables, 17, 411 (1975).

(53) R. ANNE, D. BAZIN, A.C. MUELLER, J.C. JACMART and M. LANGEVIN : Nucl. Instr. Meth. in print.

(54) J.P. DUFOUR, R. DEL MORAL, H. EMMERMANN, F. HUBERT, D. JEAN, C. POINOT, M.S. PRAVIKOFF, A. FLEURY, H. DELAGRANGE and K.H. SCHMIDT : Nucl. Instr. Meth. in Phys. Res., A248, 267 (1986).

(55) F. POUGHEON, E. QUINIOU, M. BERNAS, J.C. JACMART, S.D. HOATH, D. GUILLEMAUD-MUELLER, M.G. SAINT-LAURENT, R. ANNE, D. BAZIN, D. GUERREAU, A.C. MUELLER and C. DETRAZ : Europhys. Lett. 2, 505 (1986).

(56) D. GUILLEMAUD-MUELLER, A.C. MUELLER, D. GUERREAU, R. ANNE, C. DETRAZ, F. POUGHEON, M. BERNAS, J. GALIN, J.C. JACMART, M. LANGEVIN, F. NAULIN and E. QUINIOU : Zeitsch. für Phys. A322, 415 (1985).

(57) M. YUNO and M. YAMADA : INS report (Tokyo) NUMA 40 (1982).

(58) C. DETRAZ : 4th Int. Conf. on Nuclei far from Stability (Helsingor), CERN report 81.09, p. 261 (1981).

(59) M. LANGEVIN, M. BERNAS, J. GALIN, J.C. JACMART, F. NAULIN, F. POUGHEON, E. QUINIOU, A.C. MUELLER, D. GUILLEMAUD-MUELLER, M.G. SAINT-LAURENT,

(60) M.G. SAINT-LAURENT, J.P. DUFOUR, R. ANNE, D. BAZIN, V. BORREL, H. DELAGRANGE, C. DETRAZ, D. GUILLEMAUD-MUELLER, F. HUBERT, J.C. JACMART, A.C. MUELLER, F. POUGHEON, M.S. PRAVIKOFF and E. ROECKL : Report GANIL 87-03, and Phys. Rev. Lett. to be published.

(61) F. POUGHEON, J.C. JACMART, E. QUINIOU, R. ANNE, D. BAZIN, V. BORREL, J. GALIN, D. GUERREAU, D. GUILLEMAUD-MUELLER, A.C. MUELLER, E. ROECKL, M.G. SAINT-LAURENT and C. DETRAZ : Z. Phys., A327, 17 (1987).

(62) V.I. GOLDANSKY : Nucl. Phys., 27, 648 (1961) ; Sov. Phys. Usp., 8, 770 (1966).

(63) J. JÄNECKE : Nucl. Phys., 61, 326 (1964).

(64) V. BORREL, J.C. JACMART, F. POUGHEON, A. RICHARD, R. ANNE, D. BAZIN, H. DELAGRANGE, C. DETRAZ, J.P. DUFOUR, D. GUILLEMAUD-MUELLER, F. HUBERT, A.C. MUELLER, M.S. PRAVIKOFF, E. ROECKL and M.G. SAINT-LAURENT : to be published.

(65) L.K. PECKER, E.I. VOLMYANSKI, V.E. BUNAKOV and S.G. OGLOBLIN : Phys. Lett., 36B, 547 (1971).

(66) K.P. JACKSON, C.V. CARDINAL, H.C. EVANS, N.A. JELLEY and J. CERNY : Phys. Lett., 33B, 281 (1970).

(67) J. CERNY, J.E. ESTERL, R.A. GOUGH and R.G. SEXTRO : Phys. Lett., 33B, 284 (1979).

(68) G. AUDI, M. EPHERRE, C. THIBAULT, R. KLAPISCH, G. HUBER, F. TOUCHARD and H. WOLLNICK : AMCO 6 Conf. Nolen and Benenson ed., (Premium Press, 1979), p. 281.

(69) M. EPHERRE, G. AUDI, C. THIBAULT and R. KLAPISCH : AMCO 6 Conf., Nolen and Benenson ed., (Premium Press, 1979), p. 299.

(70) A. GILLIBERT, L. BIANCHI, B. FERNANDEZ, J. GASTEBOIS, A. CUNSOLO, A. FOTI, C. GREGOIRE, W. MITTIG, A. PEGHAIRE, Y. SCHUTZ and C. STEPHAN ; Phys. Lett., 176B, 317 (1986).

(71) A.H. WAPSTRA and G. AUDI : Nucl. Phys., A432, 1 (1985).

(72) L.K. FIFIELD, C.L. WOODS, W.N. CATFORD, R.A. BARK, P.V. DRUMM and K.T. KEOGHAN : Nucl. Phys., A453, 497 (1986).

FIGURE 1
Oisplacement of the 2 Fermi spheres for different relative velocities of the two colliding nuclei (from ref.[1])

FIGURE 2
Curves of iso-cross sections in a plot displaying the recoil velocity versus the mass of the target fragment [4]. Drastic change is observed for the system Ar + Sn from 27 MeV/u to 44 MeV/u. V_{cn} is the velocity of an hypothetical compound nucleus formed in complete fusion, is the observed average velocity of the evaporation residues.

FIGURE 3
Comparison of silicon production from 5.5 MeV/u Ar + Au, 44 MeV/u Ar + Ni and Au and 213 MeV/u Ar + C. Lines are drawn to guide the eye. The arrows, labelled 1, 2, 3 indicate the N/Z ratio for the projectile, the (Ar + Ni) and (Ar + Au) composite systems, respectively. (Taken from ref. [1]).

FIGURE 4
Invariant cross sections measured at 3° as a function of the ejectile velocity. The solid lines are calculated according to the fragmentation model.(from ref. [7]).

FIGURE 5
Ratio of the fragment to projectile velocities versus the mass of the fragment in the $^{44}Ar + {}^{68}Zn$ reaction measured at $\theta_{lab} = 3°$. The solid and dotted curves correspond to the two types of velocity described in the text (from ref. [8]).

FIGURE 6
Mass correlation between the masses of the projectile-like and target-like fragments. The solid line shows the predictions of the abrasion model (from ref.[11]).

FIGURE 7
(a) Energy-and-angle integrated mass distribution of the projectile-like fragments in the reaction $^{40}Ar + {}^{27}Al$. The lines through the data points are drawn to guide the eye. The dashed line is the mass distribution predicted by a clean-cut abrasion calculation. The solid curve represents the fragment excitation energy (right scale) predicted by the calculation of ref. [16].
(b) Ratios of the mass yields between the $^{40}Ar + {}^{nat}Ti$ and $^{40}Ar + {}^{27}Al$ reactions. The solid curve is the prediction of the clean-cut abrasion calculation. (from ref. [16])

FIGURE 8
Experimental and calculated (see text) longitudinal momentum widths as a function of the fragment mass. (from ref.[7])

FIGURE 9
Contour plots of invariant cross-sections for different ejectiles as a function of parallel and transverse velocities. The values of $d^3\sigma/dv^3$ are expressed in units of (10 mb/MeV sr)*(MeV/c). (from ref.[7]).

FIGURE 10
Evolution with energy of the experimental reduced width σ_0
a) 27 MeV/u Ar + ^{64}Zn, ref.(8)
b) 213 MeV/u Ar + ^{12}C, ref.(6).

FIGURE 11
Transverse momentum dispersions $\sigma_{\perp}$ of the projectile-like fragments as a function of their mass in the $^{40}Ar + ^{27}Al$ reaction. The values of $\sigma_{\perp}$ were deduced from a fit to the fragment angular distributions. The curves are model predictions using different values of σ_D, the transverse momentum dispersion due to the deflection of the projectile in the Coulomb and nuclear fields of the target (from ref.[16]).

FIGURE 12
The influence of the target neutron-excess is emphasized through the evolution of the measured N/Z ratio with the ejectile atomic number (ref.[10]).

FIGURE 13
Calculated final isotopic distributions for the reaction 44 A.MeV ^{40}Ar + Ta (solid lines). Comparison is made with results of ref.[5] (open circles) and those of ref.[15] (solid circles) (from ref.[12]).

FIGURE 14
Average kinetic energy per nucleon of the projectile-like fragments as a function of their mass in the reactions (a) $^{40}Ar + ^{27}Al$ and (b) $^{40}Ar + ^{nat}Ti$. Different isotopes are connected by a line. The curves labelled 1 and 3 are respectively the kinetic energy per nucleon and the excitation energy (right scale) of the primary fragments predicted by an abrasion model calculation taking into account kinematic effects. Corrections for light-particle evaporation yield curves 2 which are directly comparable to the experimental data (from ref.[16]).

FIGURE 15
Z - and A - distributions of projectile-like fragments from the reaction $^{40}Ar + ^{27}Al$ at 2.5° integrated over all energies (ref.[17]).

FIGURE 16
Energy spectra for few nucleon transfer reactions on the ^{58}Ni target nucleus. The arrows correspond to the optimum Q value prediction for each channel. The curves are theoretical DWBA predictions (ref.[18]).

FIGURE 17
Energy distributions of the projectile-like fragments detected at 5° in various coincidence configurations (from ref.[19]).

FIGURE 18
Probability of charge transfer in Ar + Ag and Ar + Au reactions (defined as the probability to find no charged particle in the forward wall in coincidence with a projectile-like fragment of charge Z_{QP} (from ref.[19])

FIGURE 19
Energy correlation for a projectile-like fragment of charge 13 detected at 4° and a coincident alpha particle detected forward (LCP stands for light coincident particle).
Two series of lines have been drawn :
. one corresponds to equal energie E^*_{α} of the alpha particle in the primary projectile-like fragment system
. the second one to equal energies E_t of the primary projectile-like

FIGURE 20
Schematic representation of the two momentum distributions of the bound state (b + c), ψ_1 and (A + c), ψ_2 separated by the total momentum change $|Q|=|k_{fc}/B+k_{ic}/a|$ (from ref. [21]).

FIGURE 21
Forbidden and allowed one-nucleon transfer in high-energy collisions (from ref. [22]).

FIGURE 22
Energy spectrum of ^{15}N fragments from the $^{16}O + ^{208}Pb$ collision. (from ref.[22]).

FIGURE 23
These inelastic scattering energy spectra provide evidence for the effectiveness of 44 MeV per nucleon ^{40}Ar projectiles to excite the giant quadrupole resonance of the target nuclei (from ref.[24]).

FIGURE 24
Inelastic scattering spectrum of the $^{12}C + ^{208}Pb$ reaction at 200 MeV per nucleon (from ref.[26]).

FIGURE 25
Inelastic spectra of $^{40}Ar + ^{90}Zr$ at 44 MeV per nucleon, around the grazing angle (from ref.[24])

FIGURE 26
An inelastic energy spectrum from $^{40}Ar + ^{90}Zn$ in the region of high excitation and its double Fourier transform (see text). (from ref.[24]

FIGURE 27
Comparison of double Fourier transforms of inelastic spectra taken over two different angular ranges. (from ref.[24])

FIGURE 28
Folding angle, θfold, between the two fission fragments in the case of complete and incomplete linear momentum transfer. V_{CN} is the velocity of the compound nucleus, V_R that of the quasi composite system (from ref. [29]).

FIGURE 29
In-plane angular correlations of fission fragments for the system $^{40}Ar + ^{232}Th$ at 31,35,39 and 44 MeV/u. Curves are drawn to guide the eye. The vertical lines at each energy correspond to θff = 170° and 110° (about 0.8 and 7 GeV/c respectively) ; the arrows indicate the location of the full momentum transfers (from ref.[30]).

FIGURE 30
Smoothed and normalized recoil energy plots for Z = 19, 17, 15 and 13 fragments produced in the collision of ^{40}Ar projectiles on ^{27}Al target nuclei. Spectra 1, 2, 3 and 4 correspond to laboratory energies of 27, 32, 36 and 40 MeV/uma, respectively. The abscissa is given in units relative to the incident beam energy (from ref.[31]).

FIGURE 31
Plot of χ^2 values as a function of energy for different values of the charge of the residue detected (see text)). (from ref.[31]).

FIGURE 32
Evolution with time of three parameters in a head-on collision of Ar (27 MeV/uma) and U, as described by Landau-Vlasov calculations [37].
a) anisotropy of the momentum distribution of nucleons
b) excitation energy in the target nucleus
c) temperature of the target nucleus
(from ref. [38])

FIGURE 33
Ar (27 MeV/uma) + U : Comparison of experimental energy spectra of particles with simulations of evaporation from fully accelerated fission fragments (- - - -), from the composite nucleus (• • • •) and the sum of these two contributions (——). The angles of the particle to the beam axis (θ) and to the spin of the emitting nucleus (Φ) are indicated. Two different types of coincidence were required to trigger these events : either the observation of two fission fragments at 55° on each side of the beam axis (upper part) or one fission fragment only at 55° (lower part). (from ref. [38]).

FIGURE 34
Decay analysis for a ^{6}Li cluster decay from the system Ar + Au at 60 MeV/u. The abscissa is the relative kinetic energy of the outgoing deuteron and alpha particle. The ordinate is the corresponding yield. The two bumps correspond to two excited states of the Li cluster.. (from ref.[42]).

FIGURE 35
Correlation functions for coincident alpha particles (a) and coincident protons and Li nuclei (b) measured for ^{40}Ar induced reactions on ^{197}Au at E/A = 60 MeV. The dashed lines indicate the extremes within which the background correlation functions were assumed to lie.(from ref.[45]).

FIGURE 36
Yield ratios N_L/N_H corresponding to the decays of ^{5}Li and ^{8}Be nuclei. The solid curves show the calculated ratios as a function of the emission temperature. The range of experimental N_L/N_H values (which depend upon the background assumptions) can be translated into a range of temperature values (from ref.[45])

FIGURE 37
The folding angle distribution of the fission fragments is given with, on top, the correlated average neutron multiplicities after efficiency corrections (from ref.[46])

FIGURE 38
The d-α correlation functions are plotted versus the relative momentum q of the two particles. A coincidence is measured with the multiplicity M of the light particles detected between 3° and 30° in a plastic wall (It is known that M decreases when the impact parameter increases). Three cases are considered :
a) without any selection in the plastic wall
b) for zero multiplicity (M = 0),
c) for M ≥ 10
A comparison is made with theoretical calculations for r_0 = 4,6 and 8 fm.(from ref. [48])

FIGURE 39
Isotopic distributions of various elements observed simultaneously in the focal plane of the LISE spectrometer (see text) from the fragmentation of ^{58}Ni projectiles. Note the very low background. The arrows indicate isotopes previously unknown. (from ref.[61])

FIGURE 40
As compared to figure 39, the use of an energy degrader between the dipoles of LISE drastically reduces the number of nuclides collected. The two-dimensional display of the energy-loss versus the time-of-flight of the observed fragments from a ^{36}Ar beam gives evidence for ^{22}Si, the first Tz = - 3 isotope ever observed. (from ref.[60])

FIGURE 41
Schematic variation with N, the neutron number, of the radioactive half lives of isotopes of given Z. So-called stable nuclei (region d) have $T_{\frac{1}{2}}$ values of the order of magnitude of the proton half life, for which only a lower limit is known. Furthermore the half lives of nuclei much heavier than ^{56}Fe are also limited by the fact that fission-like disintegration processes are open, even if it is with exceedingly long half lives. If the nucleus is bound for hadron emission but can β-decay, $T_{\frac{1}{2}}$ ranges from 1 ms up, the shortest half life yet observed being 1.5 ms for ^{35}Na. This corresponds to regions c and e, and these isotopes are usually said to "exist" or "to be bound". It is in these regions that a growing number of β-delayed emission processes have been observed. At last, if the nucleus is unbound for neutron emission, $T_{\frac{1}{2}}$ falls brutaly down to some 10^{-21} sec. A staggering odd-even effect can occur at the border of the neutron drip line. On the proton-rich side, the fall from about 10^{-3} s to 10^{-21}s is not as drastic due to the Coulomb barrier which inhibits the emission of low-energy protons. Thus, for available proton energies smaller than about 1 MeV (region b) proton radioactivity can take place and was actually observed. That is also where two-protons radioactivity is expected. The limit between this region b and region a were unbound protons leave the nucleus before it is actually observed obviously depends upon detection techniques. Hence the limit between proton-active and proton-unbound nuclei cannot be but somewhat arbitrary. It should be emphasized that, for most Z values, except the very lowest ones, only a small fraction of this curve is known.

FIGURE 42
An analysis of the deviation of the absolute masses of known nuclei as measured at GANIL where m_g refers to the measured value and m_w to the compilation by Wapstra and Audi[71]. The dispersion of the values around zero has a FWHM of 4×10^{-5} (from ref.[70]).

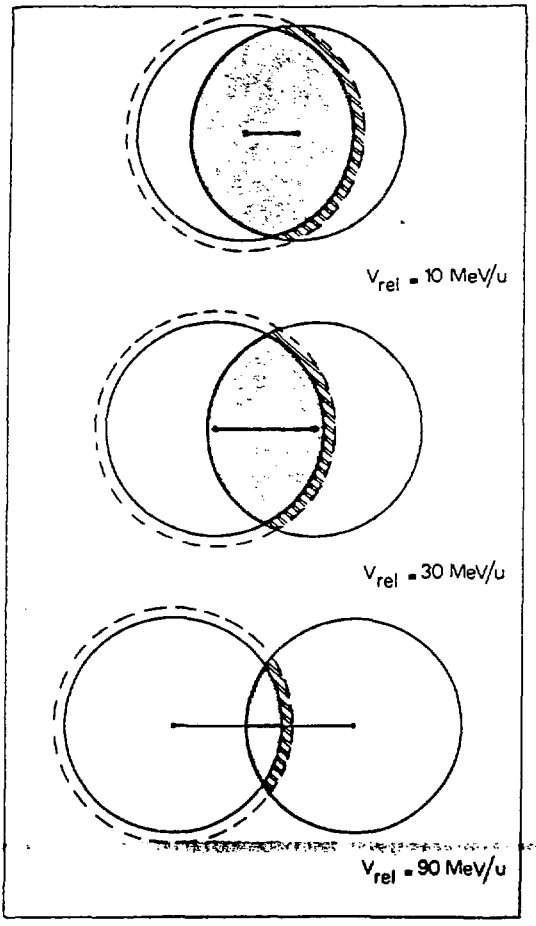

Fig. 1

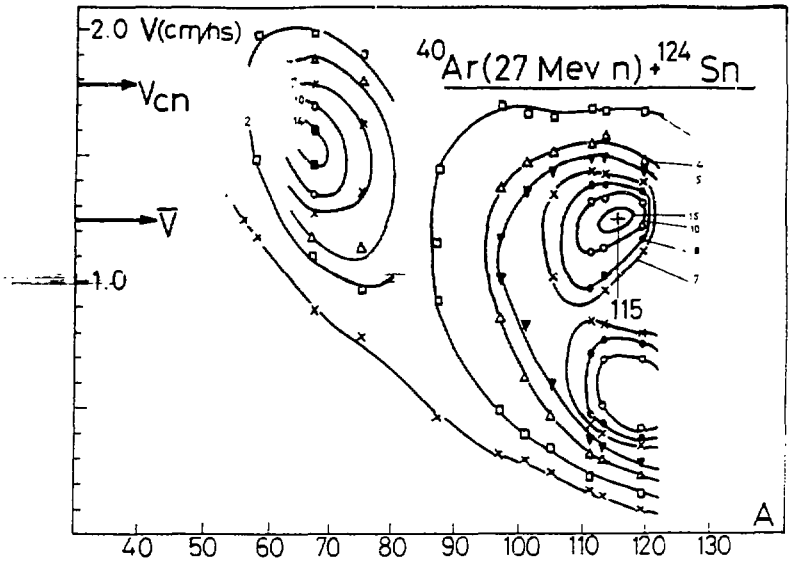
2.0 V(cm/ns)
Vcn
V̄
1.0
40Ar(27 Mev n)+124Sn
115
A
40 50 60 70 80 90 100 110 120 130

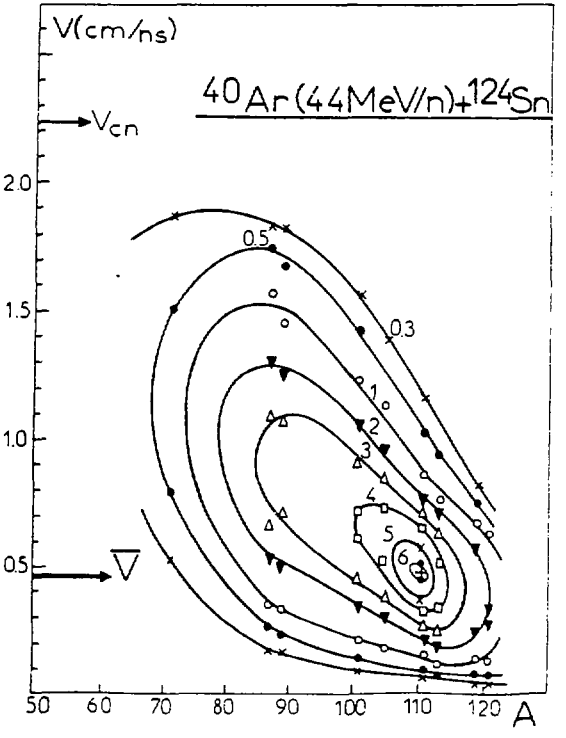
V(cm/ns)
40Ar(44MeV/n)+124Sn
Vcn
2.0
1.5
1.0
0.5
V̄
0.5
0.3
1
2
3
4
5
6
50 60 70 80 90 100 110 120
A

Fig. 2

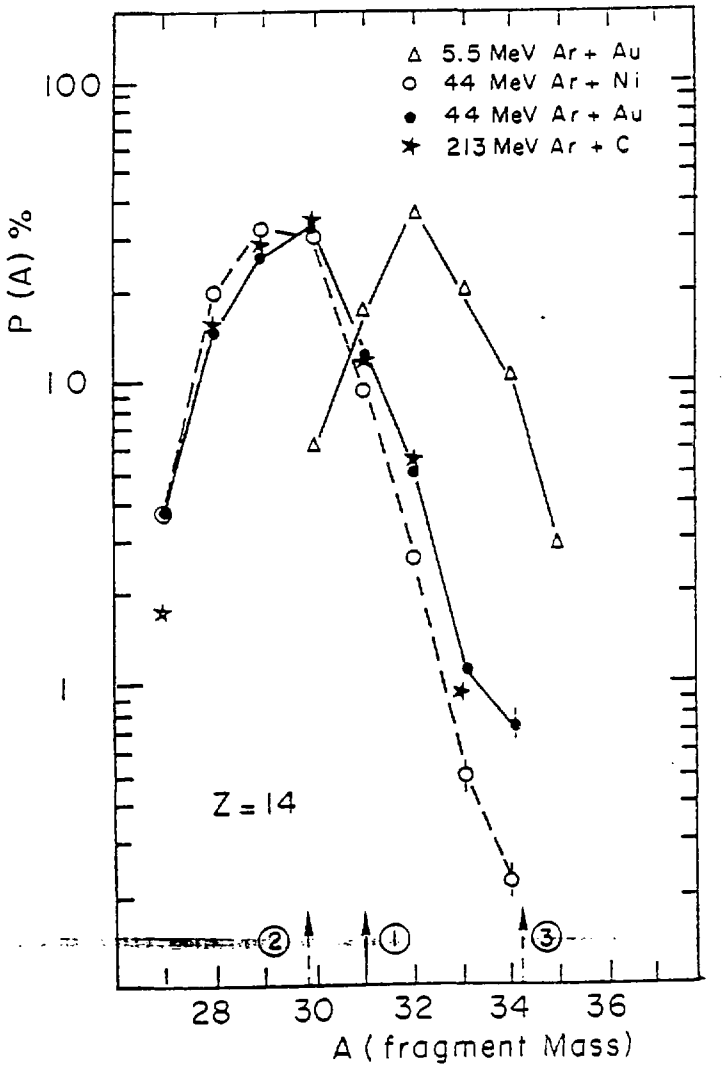
5.5 MeV Ar + Au
44 MeV Ar + Ni
44 MeV Ar + Au
213 MeV Ar + C
100
10
1
P (A) %
Z = 14
2
1
3
28
30
32
34
36
A (fragment Mass)

Fig. 3

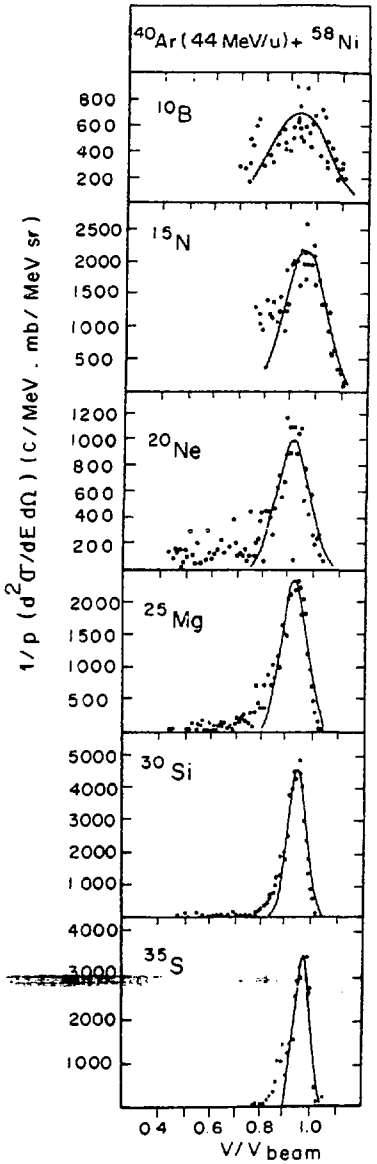
^{40}Ar (44 MeV/u) + ^{58}Ni
^{10}B
^{15}N
^{20}Ne
^{25}Mg
^{30}Si
^{35}S
1/p (d^{2}σ/dE dΩ) (c/MeV . mb/MeV sr)
V/V beam
0.4
0.6
0.8
1.0

Fig. 4

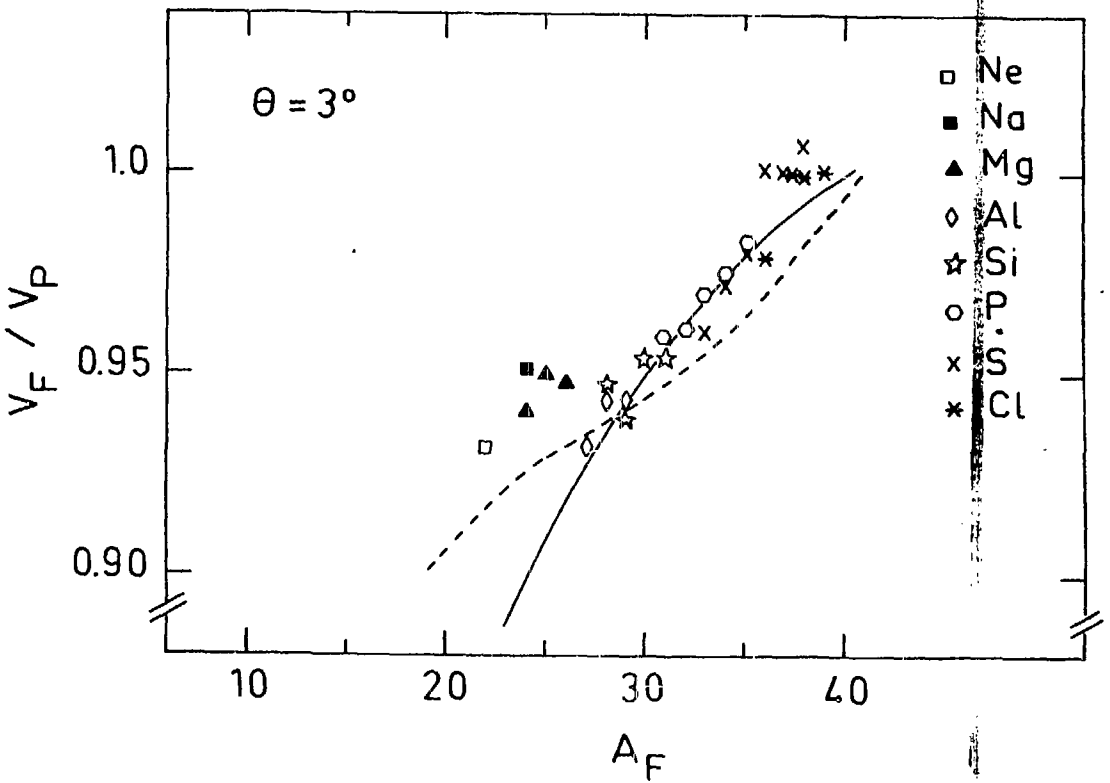

Fig. 5

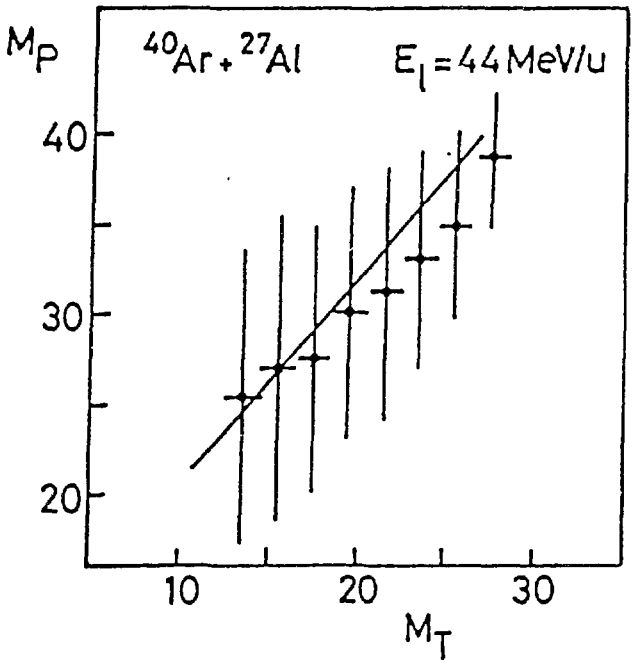

Fig. 6

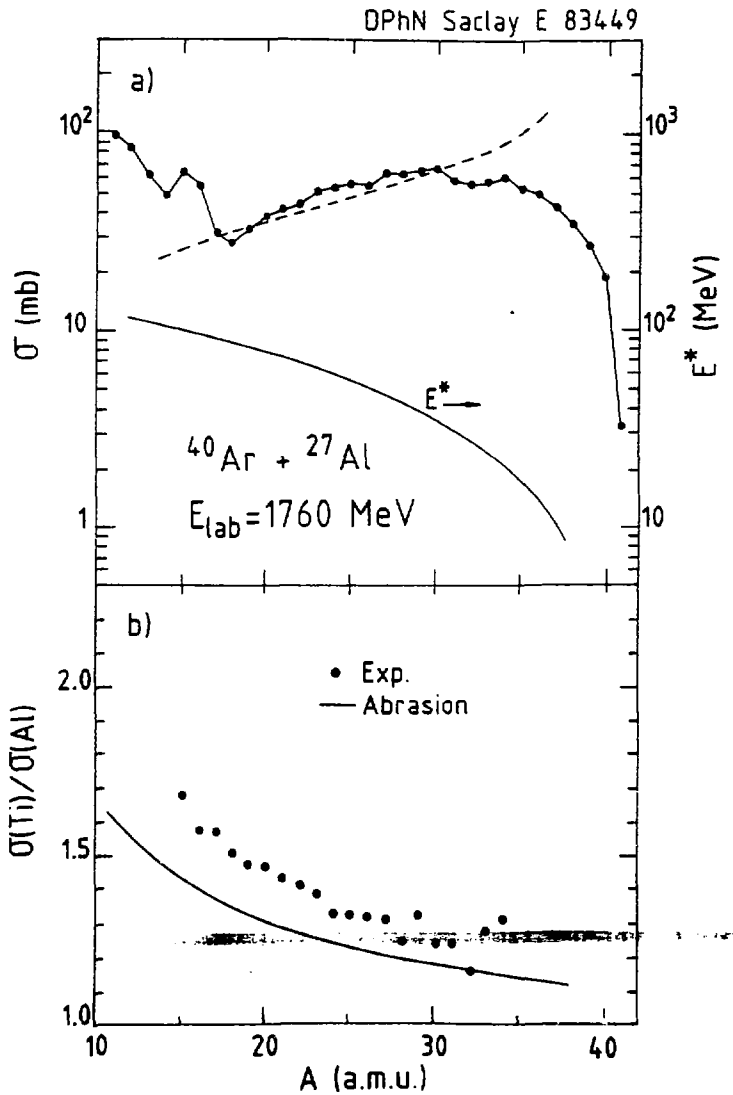
DPhN Saclay E 83449
a)
10^2
10
1
10^3
10^2
10
σ (mb)
E* (MeV)
E*
$^{40}Ar + ^{27}Al$
E_{lab}=1760 MeV
b)
• Exp.
— Abrasion
2.0
1.5
1.0
σ(Ti)/σ(Al)
10
20
30
40
A (a.m.u.)

Fig. 7

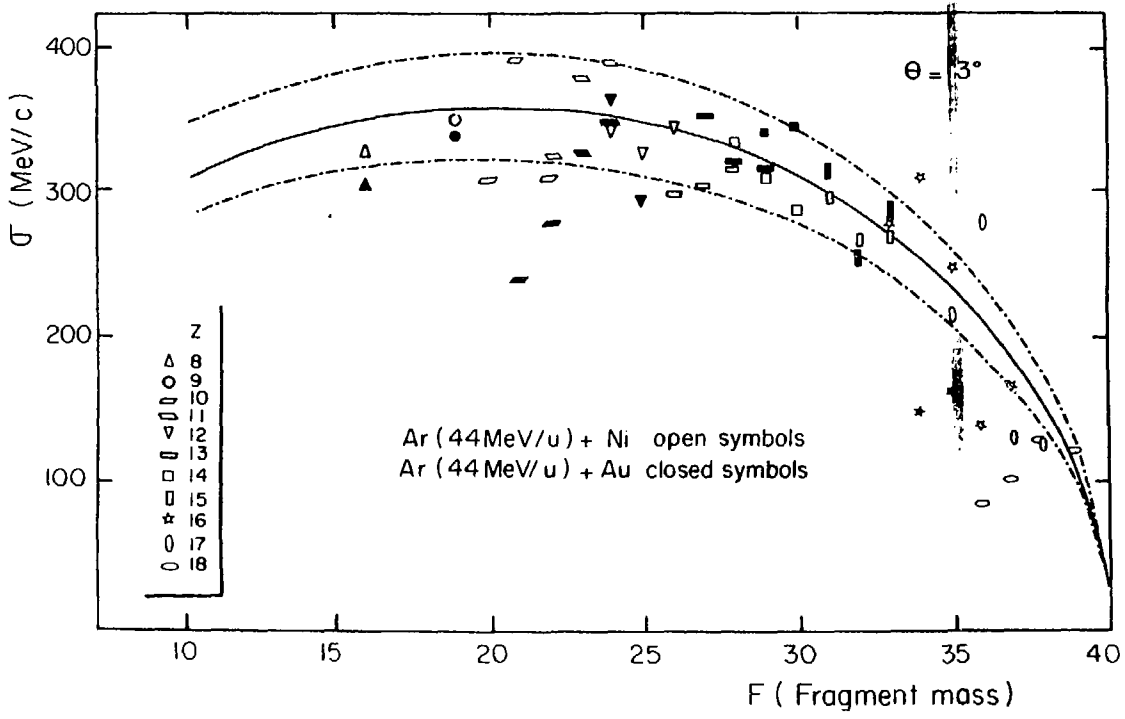
σ (MeV/c)
400
300
200
100
10
15
20
25
30
35
40
F (Fragment mass)
Θ = 3°
Z
8
9
10
11
12
13
14
15
16
17
18
Ar (44MeV/u) + Ni open symbols
Ar (44MeV/u) + Au closed symbols

Fig. 8

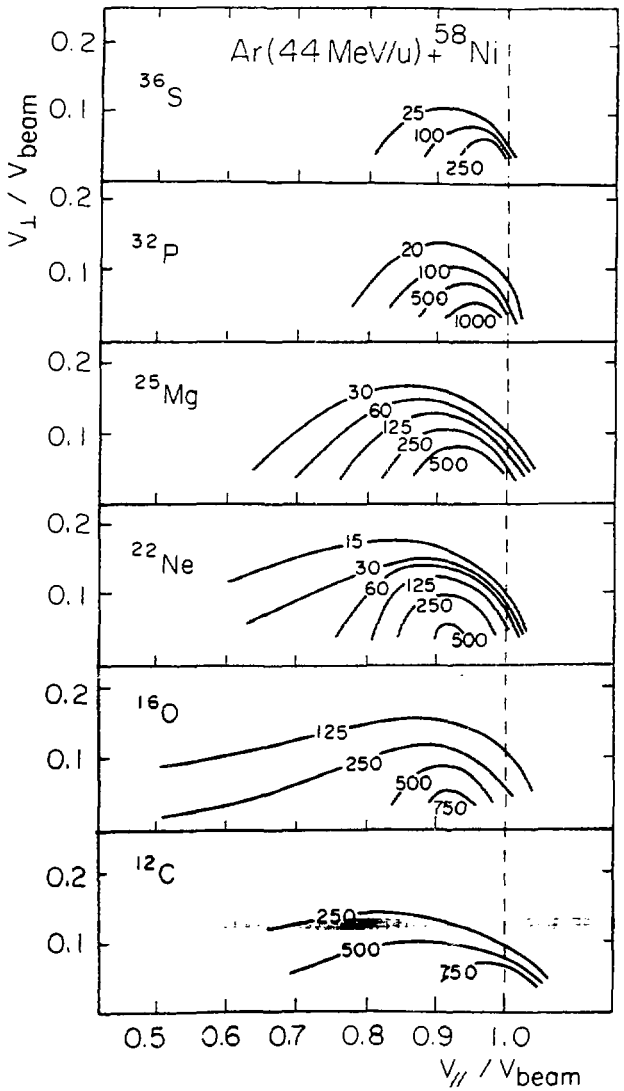
Ar(44 MeV/u) + 58Ni
36S
25
100
250
32P
20
100
500
1000
25Mg
30
60
125
250
500
22Ne
15
30
60
125
250
500
16O
125
250
500
750
12C
250
500
750
0.2
0.1
0.5
0.6
0.7
0.8
0.9
1.0
V⊥ / Vbeam
V// / Vbeam

Fig. 9

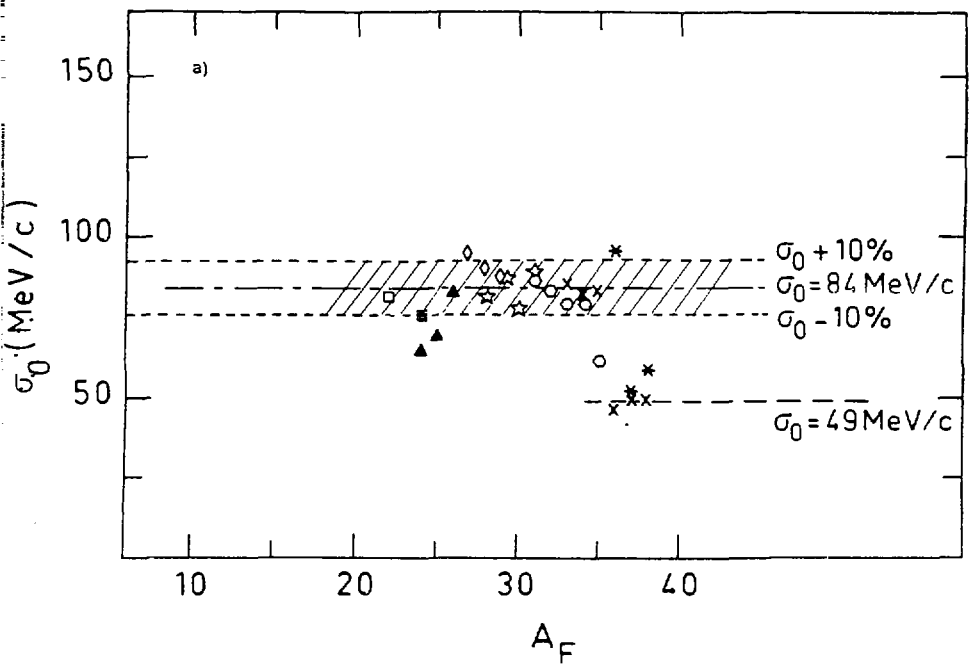
a)
150
100
50
σ_0 (MeV/c)
σ_0 + 10%
σ_0 = 84 MeV/c
σ_0 - 10%
σ_0 = 49 MeV/c
10
20
30
40
A_F

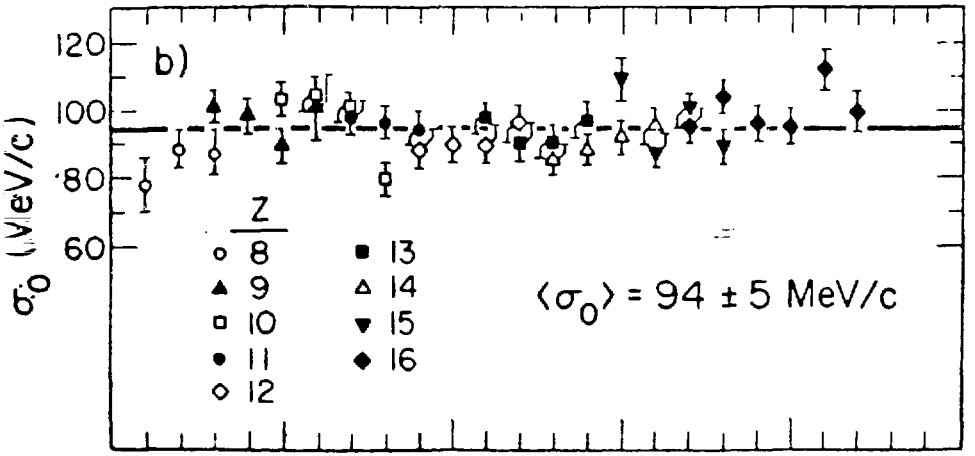
b)
120
100
80
60
σ_0 (MeV/c)
Z
8
9
10
11
12
13
14
15
16
$\langle\sigma_0\rangle$ = 94 ± 5 MeV/c

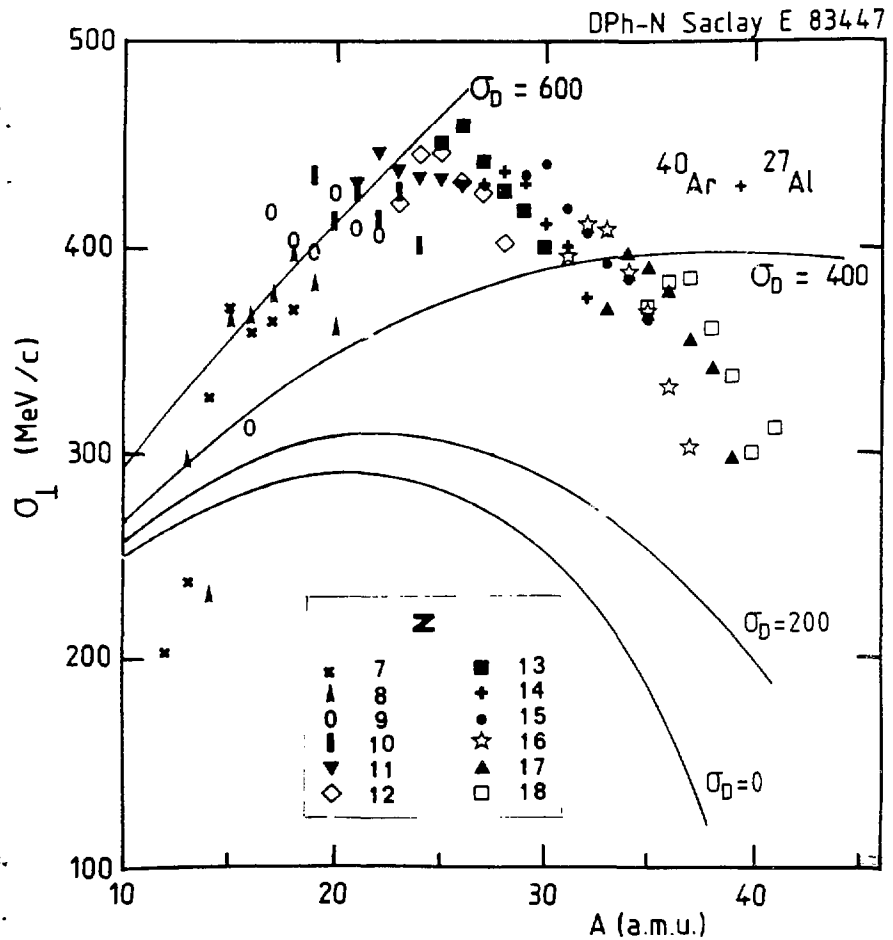
DPh-N Saclay E 83447
σ_D = 600
^{40}Ar + ^{27}Al
σ_D = 400
σ_D=200
σ_D=0
Z
7
8
9
10
11
12
13
14
15
16
17
18
$\sigma_\perp$ (MeV/c)
A (a.m.u.)
500
400
300
200
100
10
20
30
40

Fig. 11

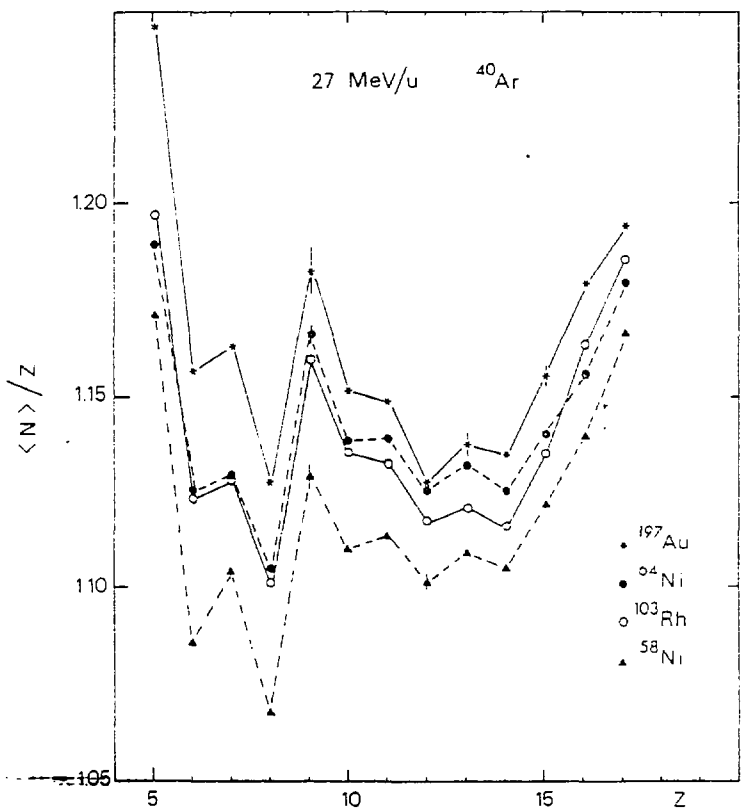

Fig. 12

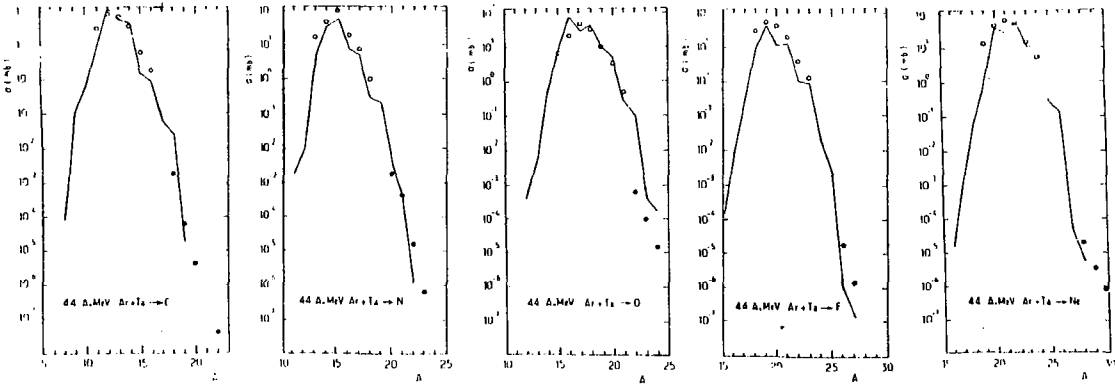
44 A.MeV Ar+Ta → F
44 A.MeV Ar+Ta → N
44 A.MeV Ar+Ta → O
44 A.MeV Ar+Ta → F
44 A.MeV Ar+Ta → Ne
A

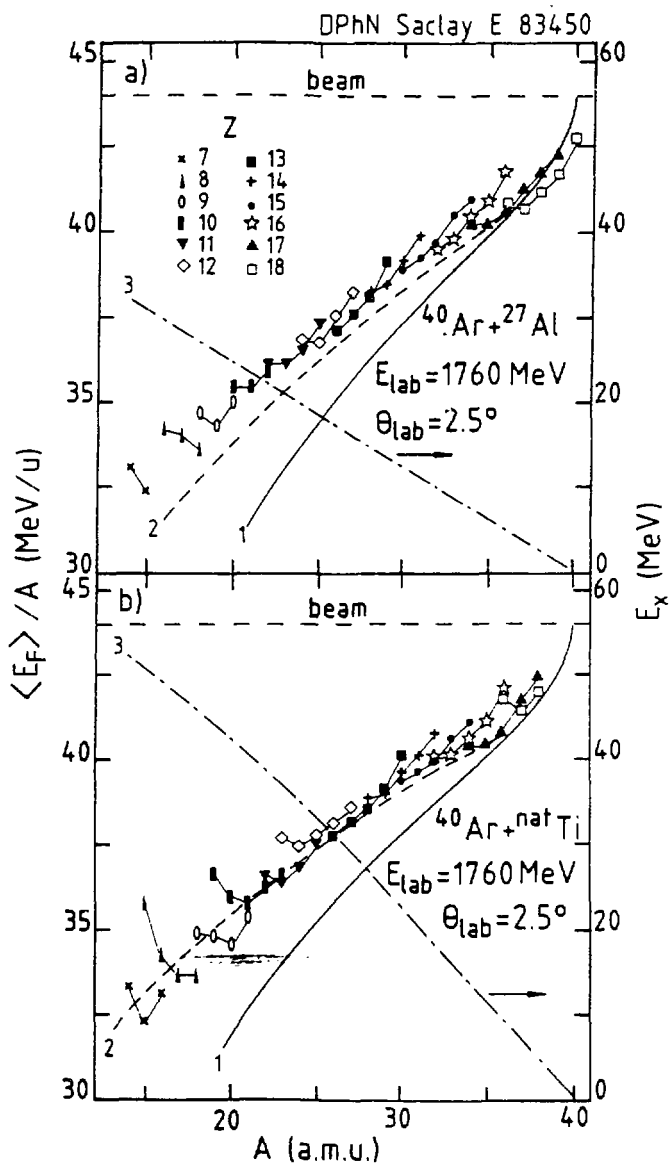
DPhN Saclay E 83450
a)
beam
Z
7
8
9
10
11
12
13
14
15
16
17
18
$^{40}Ar+^{27}Al$
E_{lab}=1760 MeV
θ_{lab}=2.5°
b)
beam
$^{40}Ar+^{nat}Ti$
E_{lab}=1760 MeV
θ_{lab}=2.5°
1
2
3
$\langle E_F \rangle$ /A (MeV/u)
E_x (MeV)
A (a.m.u.)
30
35
40
45
0
20
40
60

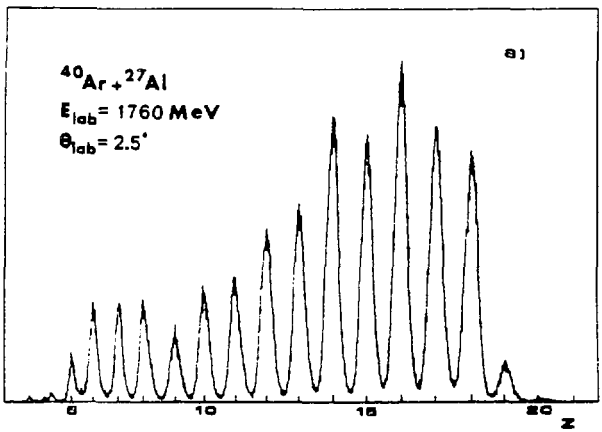
a)
$^{40}Ar + ^{27}Al$
E_{lab} = 1760 MeV
θ_{lab} = 2.5°
0
10
15
20
Z

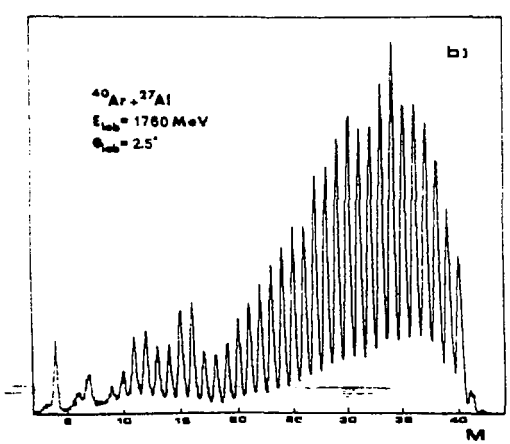
b)
$^{40}Ar + ^{27}Al$
E_{lab} = 1760 MeV
θ_{lab} = 2.5°
M

Fig. 15

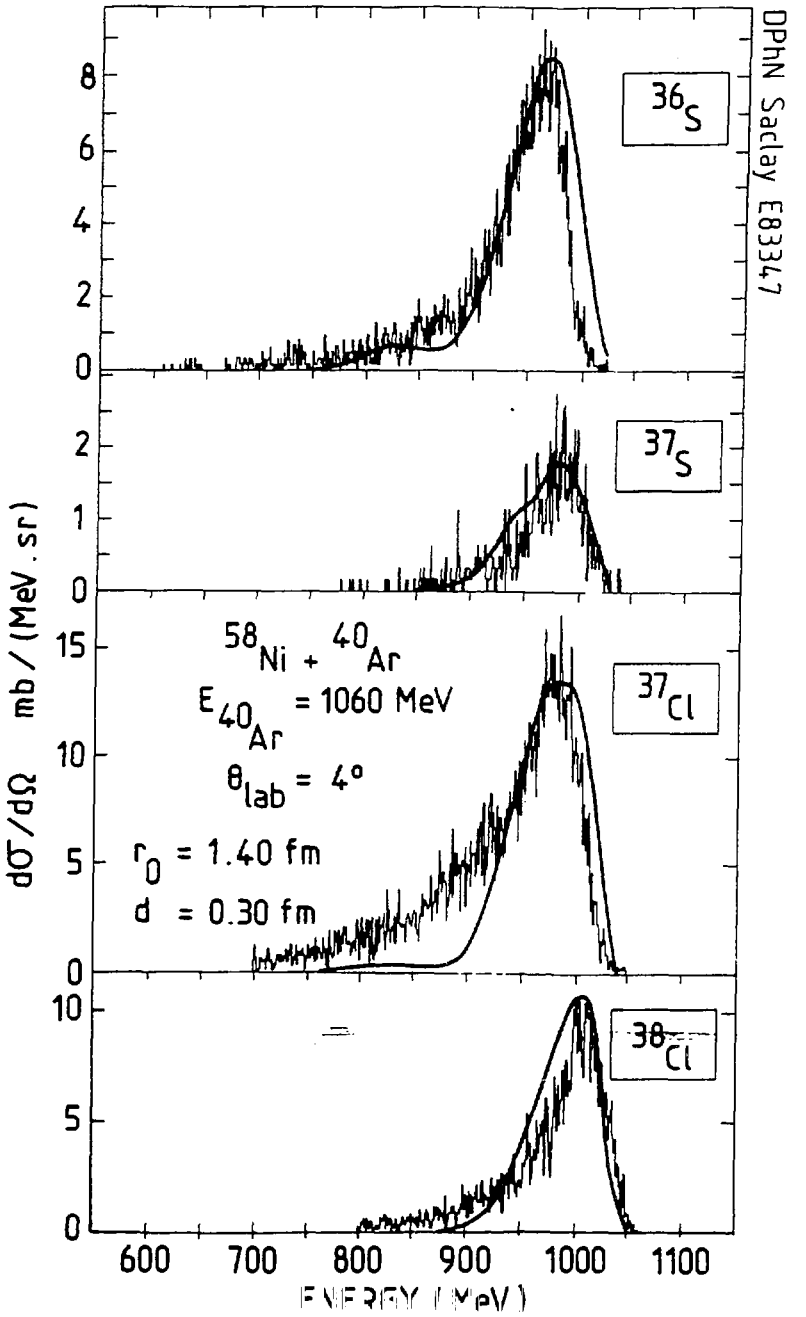
DPhN Saclay E83347
36S
37S
37Cl
38Cl
58Ni + 40Ar
E40Ar = 1060 MeV
θlab = 4°
r0 = 1.40 fm
d = 0.30 fm
dσ/dΩ mb/(MeV.sr)
ENERGY (MeV)
600
700
800
900
1000
1100

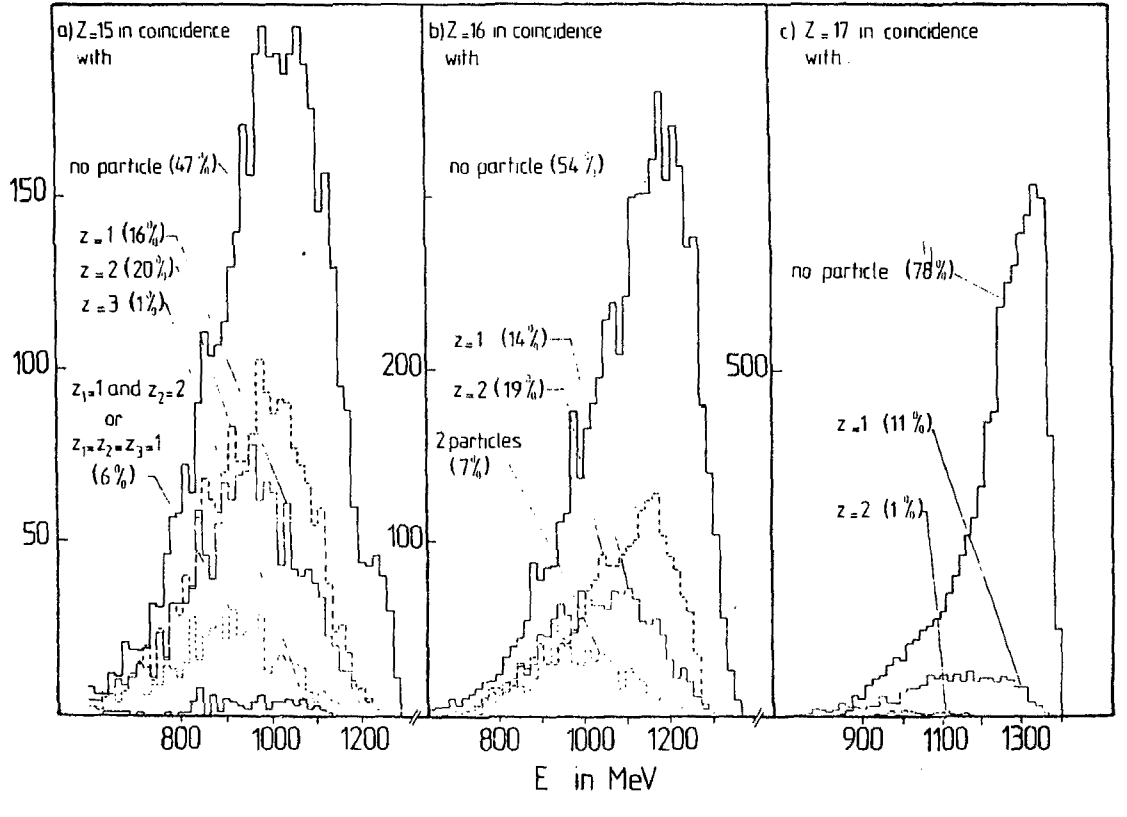
a) Z=15 in coincidence with
no particle (47 %)
z=1 (16%)
z=2 (20%)
z=3 (1%)
z1=1 and z2=2 or z1=z2=z3=1 (6%)
150
100
50
800
1000
1200
b) Z=16 in coincidence with
no particle (54 %)
z=1 (14%)
z=2 (19%)
2 particles (7%)
200
100
800
1000
1200
c) Z=17 in coincidence with
no particle (78%)
z=1 (11%)
z=2 (1%)
500
900
1100
1300
E in MeV

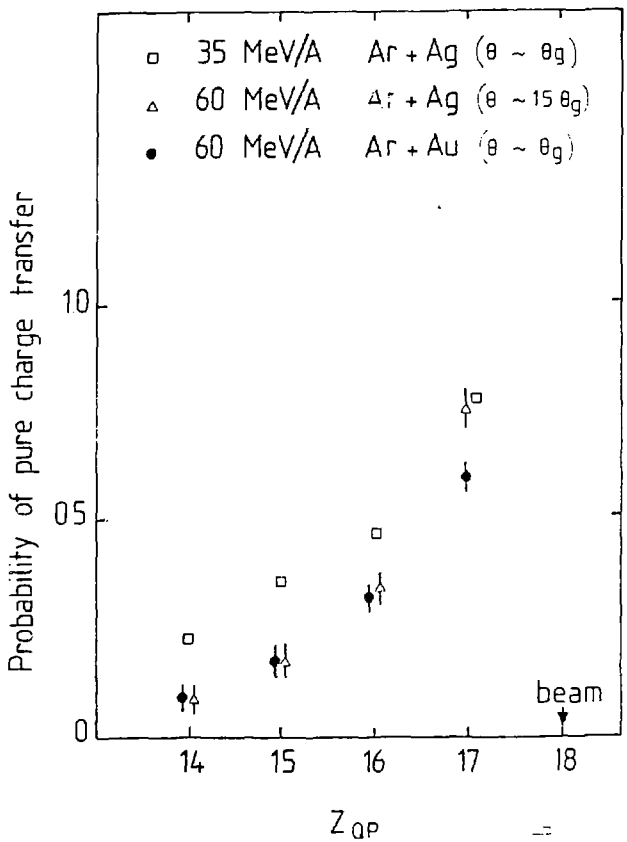
35 MeV/A Ar + Ag (θ ~ θg)
60 MeV/A Ar + Ag (θ ~ 15 θg)
60 MeV/A Ar + Au (θ ~ θg)
Probability of pure charge transfer
1.0
0.5
0
beam
14
15
16
17
18
Z QP

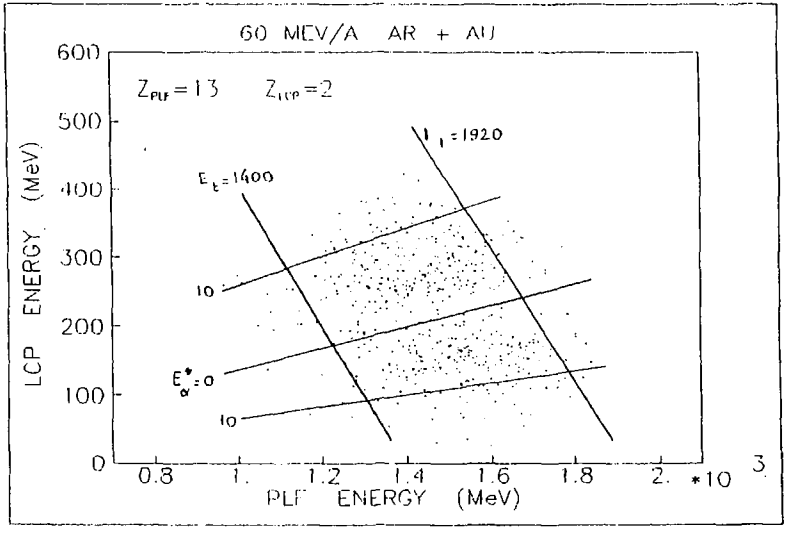
60 MEV/A AR + AU
$Z_{PLF}=13$
$Z_{LCP}=2$
$I_1=1920$
$E_t=1400$
10
$E^*_\alpha=0$
10
LCP ENERGY (MeV)
600
500
400
300
200
100
0
0.8
1.
1.2
1.4
1.6
1.8
2.
*10 3
PLF ENERGY (MeV)

Fig. 19

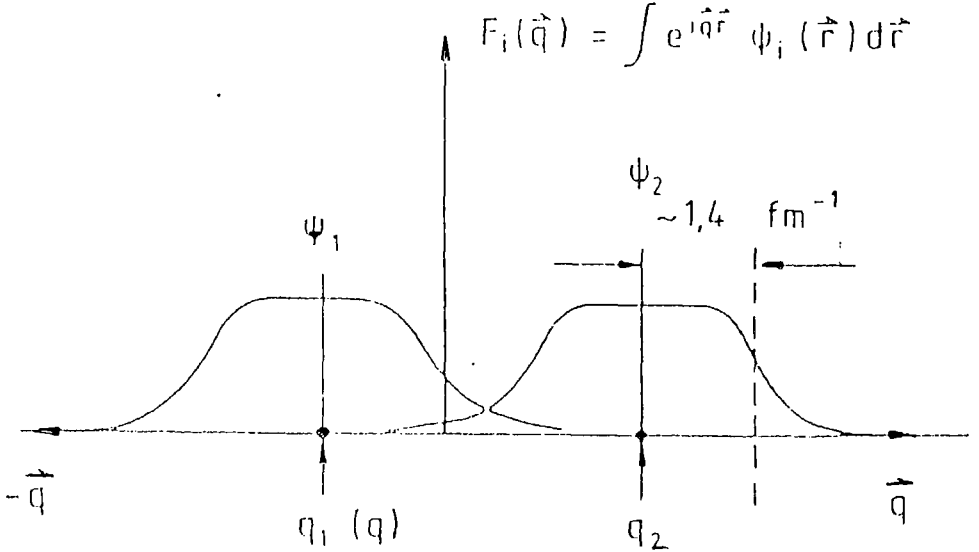
$F_i(\vec{q}) = \int e^{i\vec{q}\vec{r}}\ \psi_i(\vec{r})\, d\vec{r}$
ψ_2
$\sim 1{,}4$ fm^{-1}
ψ_1
$-\vec{q}$
q_1 (q)
q_2
$\vec{q}$

DPhN Saclay E 83583

$j_{i<} = 1p1/2 = l_i - 1/2$

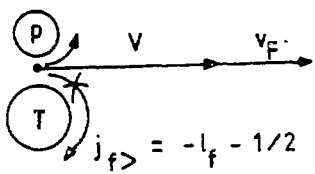

FORBIDDEN

$j_{i<} = 1p1/2 = -l_i + 1/2$

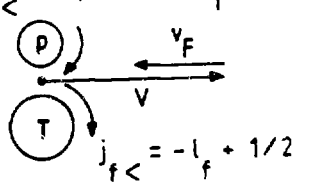

ALLOWED

Fig. 21

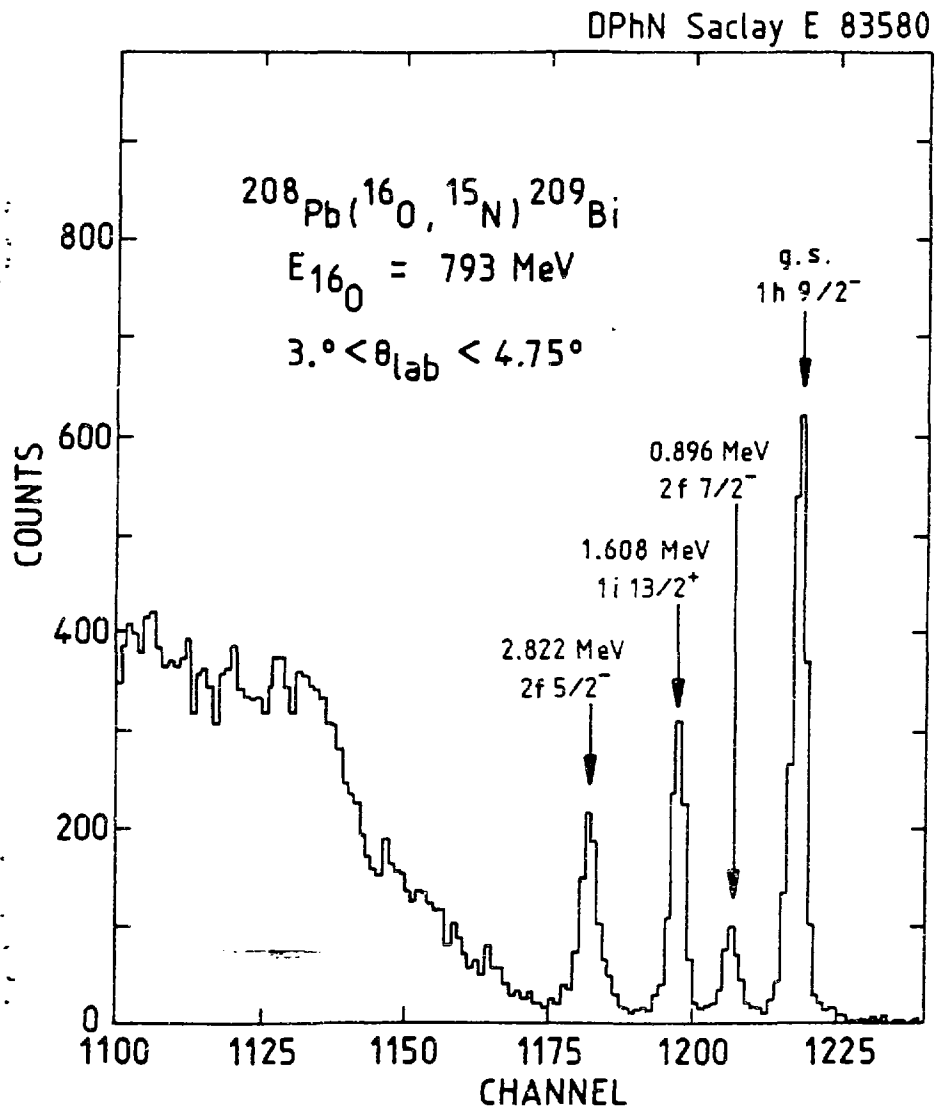
DPhN Saclay E 83580
$^{208}Pb(^{16}O, ^{15}N)^{209}Bi$
$E_{^{16}O}$ = 793 MeV
$3.° < \theta_{lab} < 4.75°$
g.s.
1h 9/2⁻
0.896 MeV
2f 7/2⁻
1.608 MeV
1i 13/2⁺
2.822 MeV
2f 5/2⁻
COUNTS
CHANNEL
0
200
400
600
800
1100
1125
1150
1175
1200
1225

Fig. 22

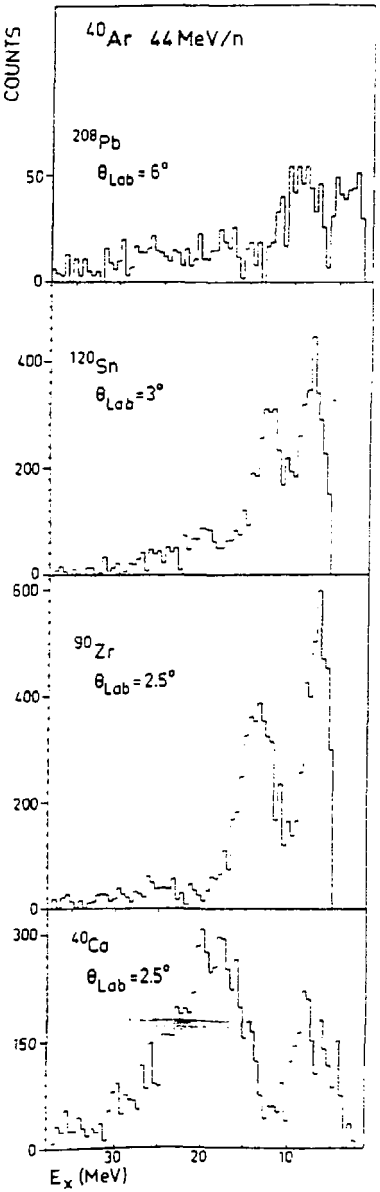
COUNTS
40Ar 44MeV/n
208Pb
θLab = 6°
50
0
120Sn
θLab = 3°
400
200
0
90Zr
θLab = 2.5°
600
400
200
0
40Ca
θLab = 2.5°
300
150
0
30
20
10
Ex (MeV)

Fig. 23

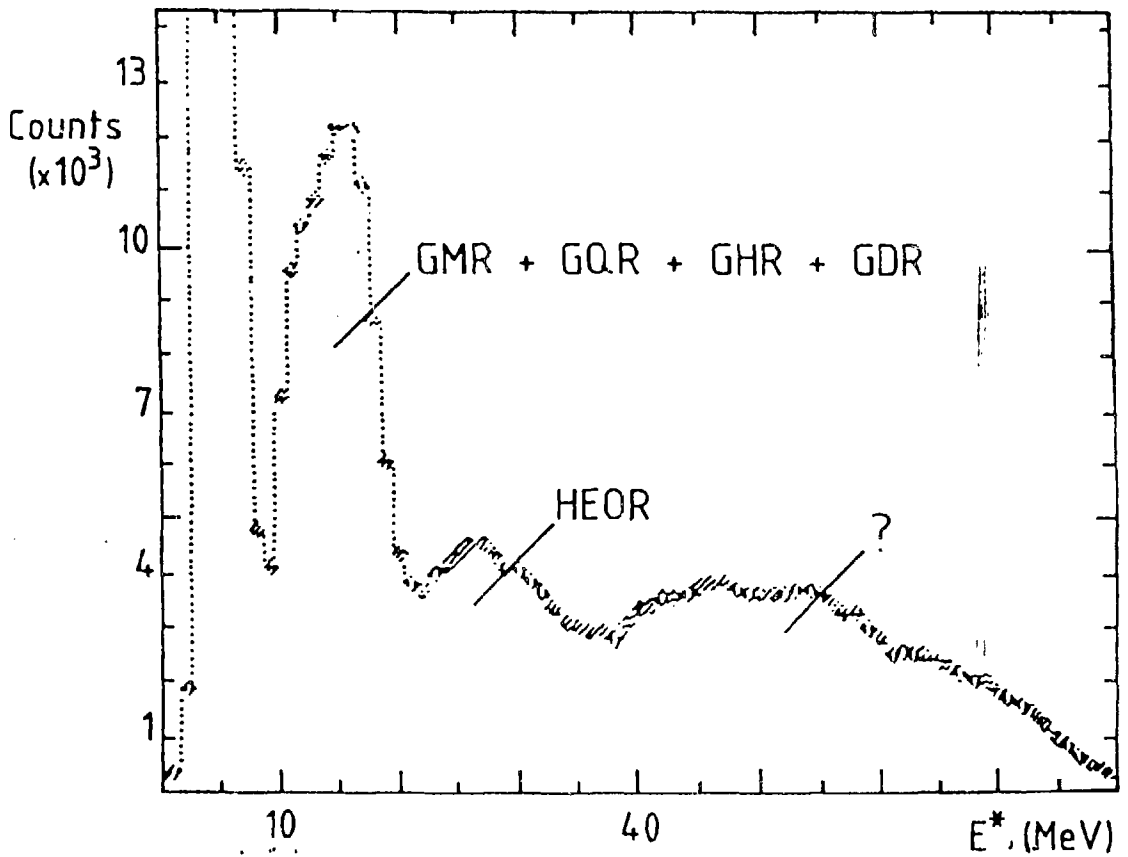

Fig. 24

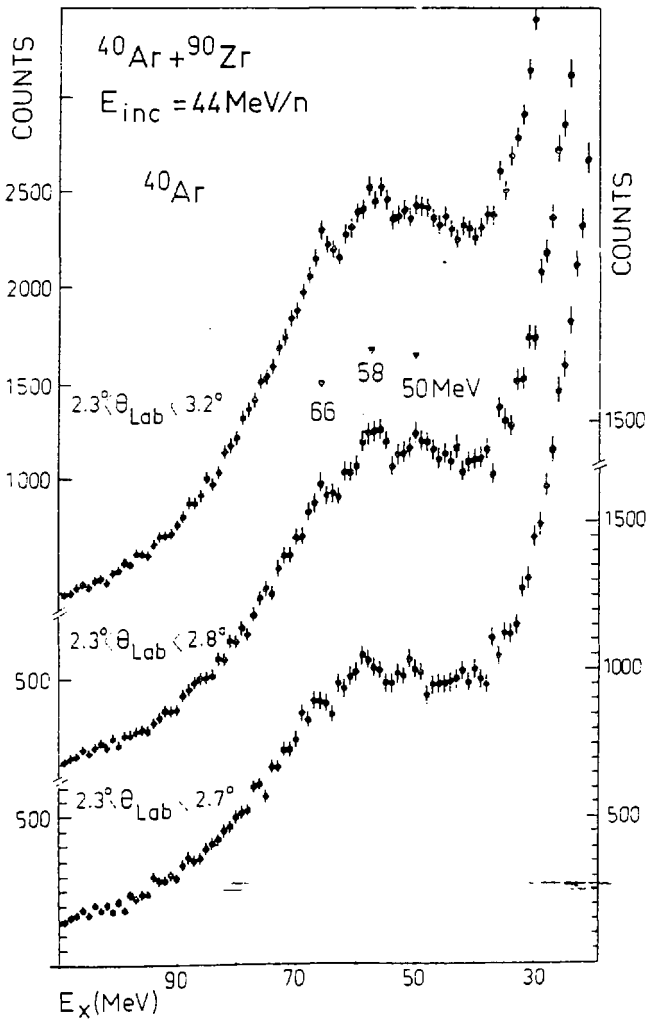
$^{40}Ar + ^{90}Zr$
$E_{inc} = 44 MeV/n$
^{40}Ar
COUNTS
2500
2000
1500
1000
500
500
$2.3° \leq \theta_{Lab} \leq 3.2°$
$2.3° \leq \theta_{Lab} \leq 2.8°$
$2.3° \leq \theta_{Lab} \leq 2.7°$
58
66
50 MeV
1500
1500
1000
500
90
70
50
30
E_x(MeV)

Fig. 25

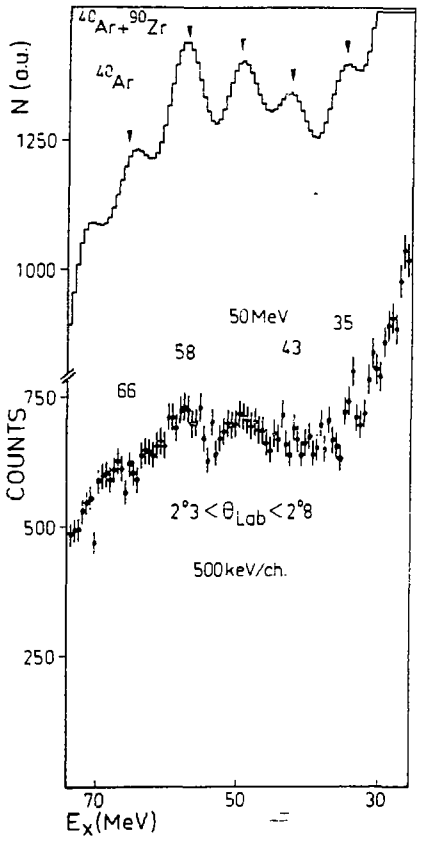
$^{40}Ar+^{90}Zr$
^{40}Ar
N (a.u.)
1250
1000
750
500
250
50 MeV
35
58
43
66
COUNTS
$2°3 < \theta_{Lab} < 2°8$
500 keV/ch.
70
50
30
E_x(MeV)

Fig. 26

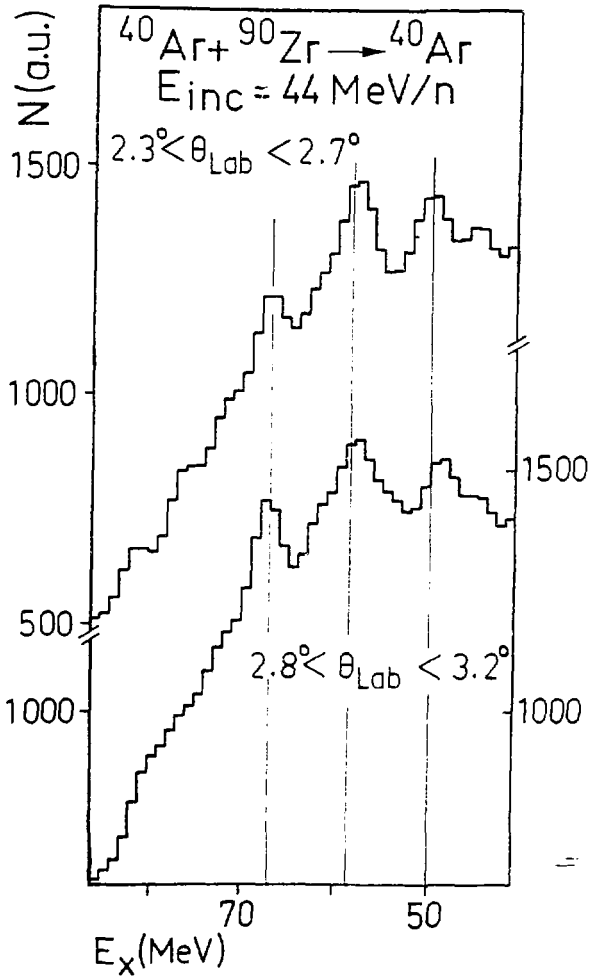
$^{40}Ar + ^{90}Zr \rightarrow ^{40}Ar$
$E_{inc} \approx 44$ MeV/n
$2.3° < \theta_{Lab} < 2.7°$
$2.8° < \theta_{Lab} < 3.2°$
N(a.u.)
1500
1000
500
1000
1500
1000
70
50
E_x(MeV)

Fig. 27

Complete linear momentum transfer

$$V_{CN} = \frac{A_1}{A_1 + A_2} v_1$$

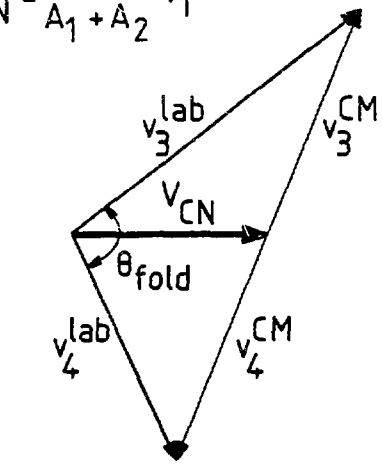

Incomplete linear momentum transfer

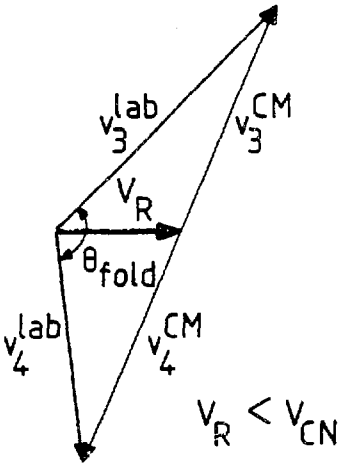

Fig. 28

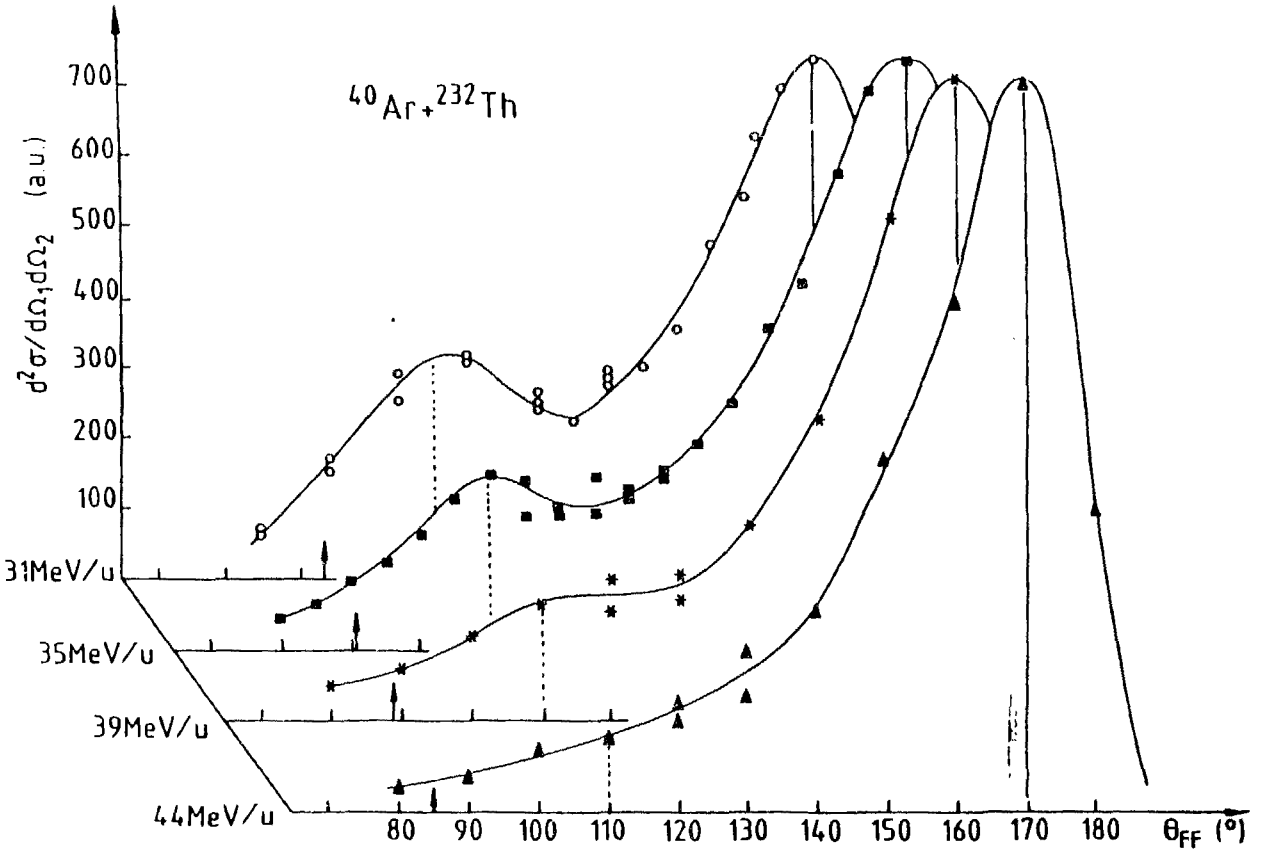
$^{40}Ar + ^{232}Th$
$d^2\sigma/d\Omega_1 d\Omega_2$ (a.u.)
700
600
500
400
300
200
100
31MeV/u
35MeV/u
39MeV/u
44MeV/u
80
90
100
110
120
130
140
150
160
170
180
θ_{FF} (°)

Fig. 29

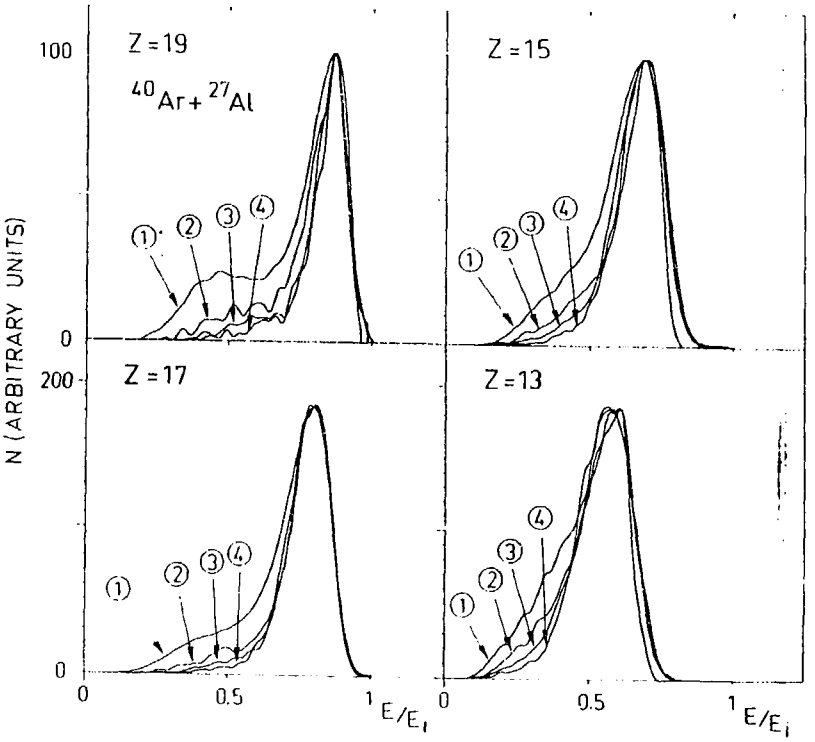
Z = 19
$^{40}Ar + ^{27}Al$
Z = 15
Z = 17
Z = 13
N (ARBITRARY UNITS)
100
0
200
0
0.5
1
E/E_i
①
②
③
④

Fig. 30

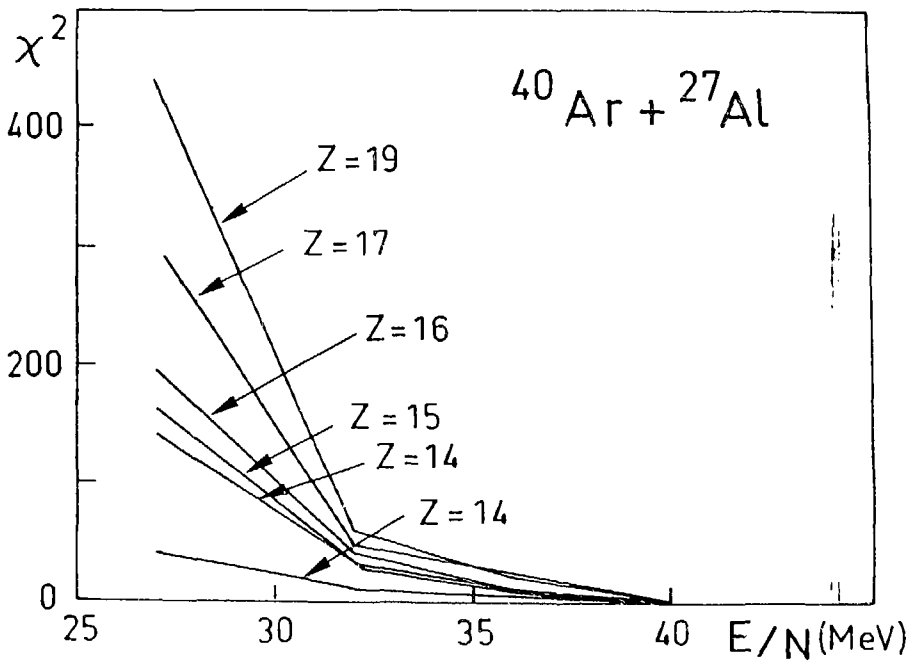
χ^2
400
200
0
25
30
35
40
E/N(MeV)
$^{40}Ar + ^{27}Al$
Z = 19
Z = 17
Z = 16
Z = 15
Z = 14
Z = 14

Fig. 31

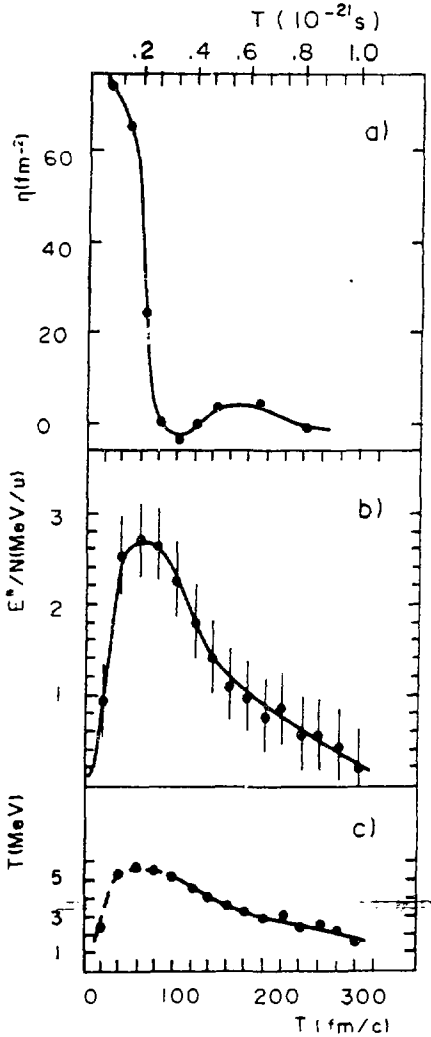
T (10^-21 s)
.2
.4
.6
.8
1.0
a)
η(fm^-2)
60
40
20
0
b)
E*/N(MeV/u)
3
2
1
c)
T(MeV)
5
3
1
0
100
200
300
T (fm/c)

Fig. 32

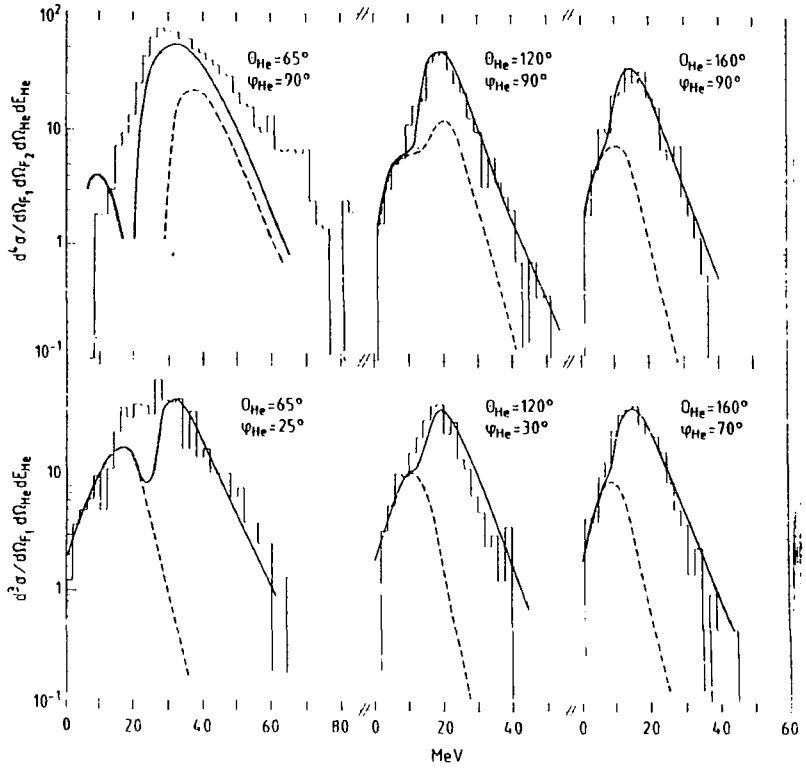
10^2
10
1
10^{-1}
$d^4\sigma/d\Omega_{F_1}\,d\Omega_{F_2}\,d\Omega_{He}\,dE_{He}$
$\theta_{He}=65°$
$\varphi_{He}=90°$
$\theta_{He}=120°$
$\varphi_{He}=90°$
$\theta_{He}=160°$
$\varphi_{He}=90°$
$d^3\sigma/d\Omega_{F_1}\,d\Omega_{He}\,dE_{He}$
$\theta_{He}=65°$
$\varphi_{He}=25°$
$\theta_{He}=120°$
$\varphi_{He}=30°$
$\theta_{He}=160°$
$\varphi_{He}=70°$
0
20
40
60
80
MeV

Fig. 33

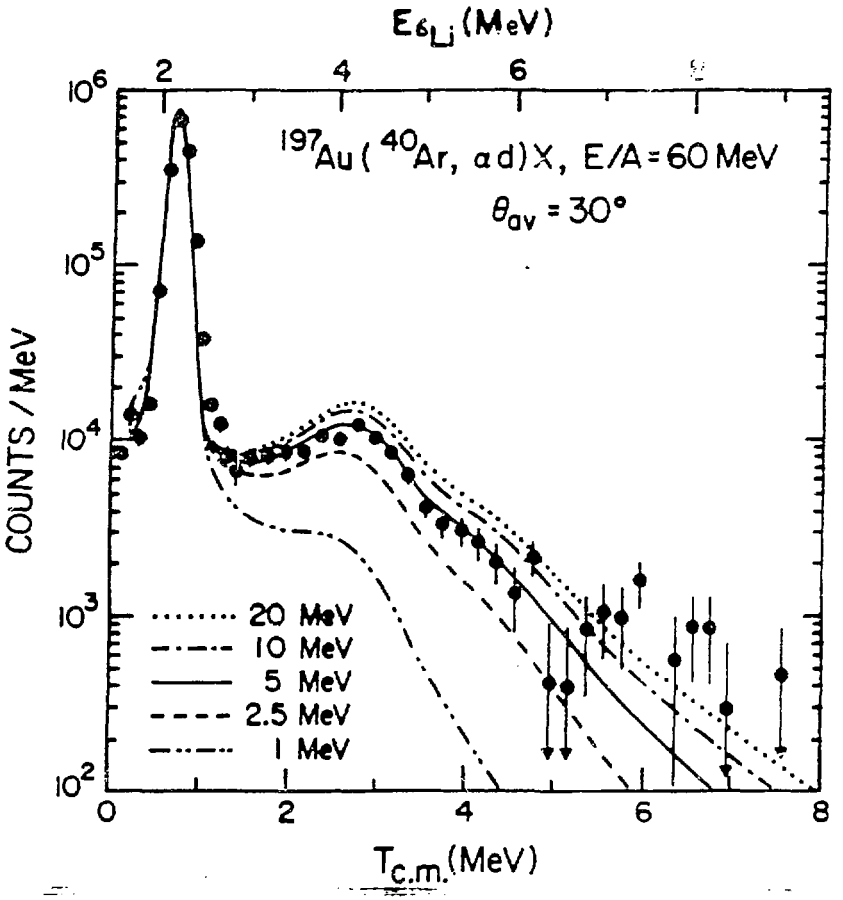
$E_{^6Li}$ (MeV)
2
4
6
10^6
10^5
10^4
10^3
10^2
$^{197}Au(^{40}Ar, \alpha d)X$, E/A = 60 MeV
$\theta_{av} = 30°$
COUNTS / MeV
20 MeV
10 MeV
5 MeV
2.5 MeV
1 MeV
0
2
4
6
8
$T_{c.m.}$ (MeV)

Fig. 34

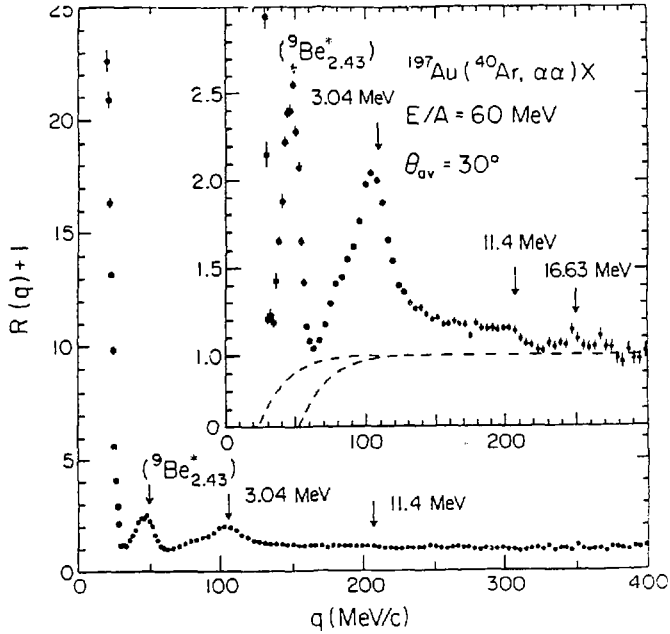
($^{9}Be^{*}_{2.43}$)
3.04 MeV
$^{197}Au(^{40}Ar, \alpha\alpha)X$
E/A = 60 MeV
θ_{av} = 30°
11.4 MeV
16.63 MeV
($^{9}Be^{*}_{2.43}$)
3.04 MeV
11.4 MeV
R(q)+1
q (MeV/c)

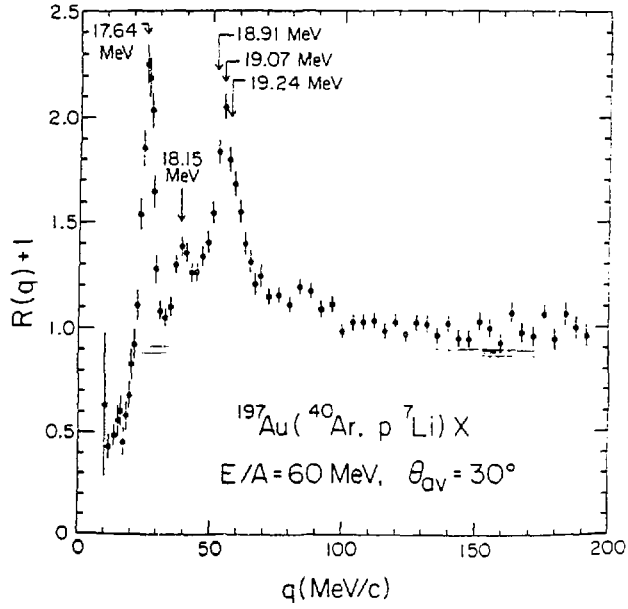
17.64 MeV
18.91 MeV
19.07 MeV
19.24 MeV
18.15 MeV
$^{197}Au(^{40}Ar, p\ ^{7}Li)X$
E/A = 60 MeV, θ_{av} = 30°
R(q)+1
q(MeV/c)

Fig. 35

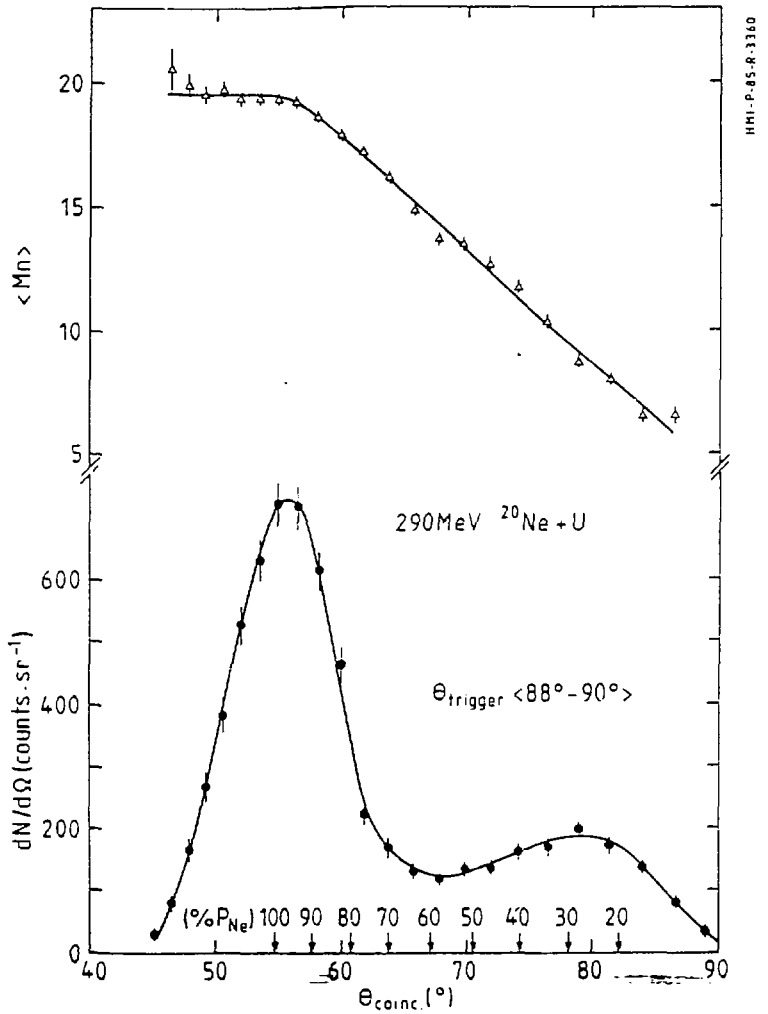
HMI-P-85-A-3360
<Mn>
20
15
10
5
290MeV ^{20}Ne + U
$\theta_{trigger}$ <88°-90°>
dN/dΩ (counts·sr^{-1})
600
400
200
0
(%P_{Ne}) 100 90 80 70 60 50 40 30 20
40
50
60
70
80
90
$\theta_{coinc.}$ (°)

Fig. 57

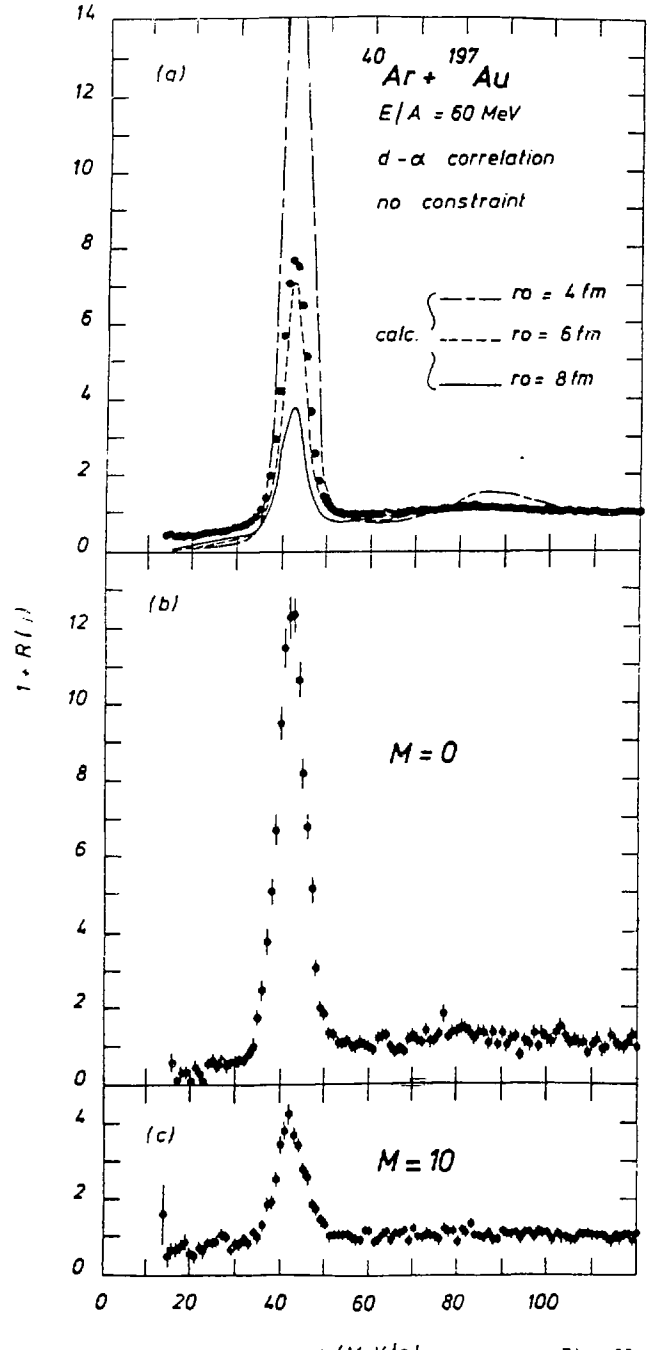
(a)
40 Ar + 197 Au
E/A = 60 MeV
d - α correlation
no constraint
calc. ro = 4 fm
ro = 6 fm
ro = 8 fm
(b)
M = 0
(c)
M = 10
1 + R(q)
q (MeV/c)

Fig. 38

Fig. 39

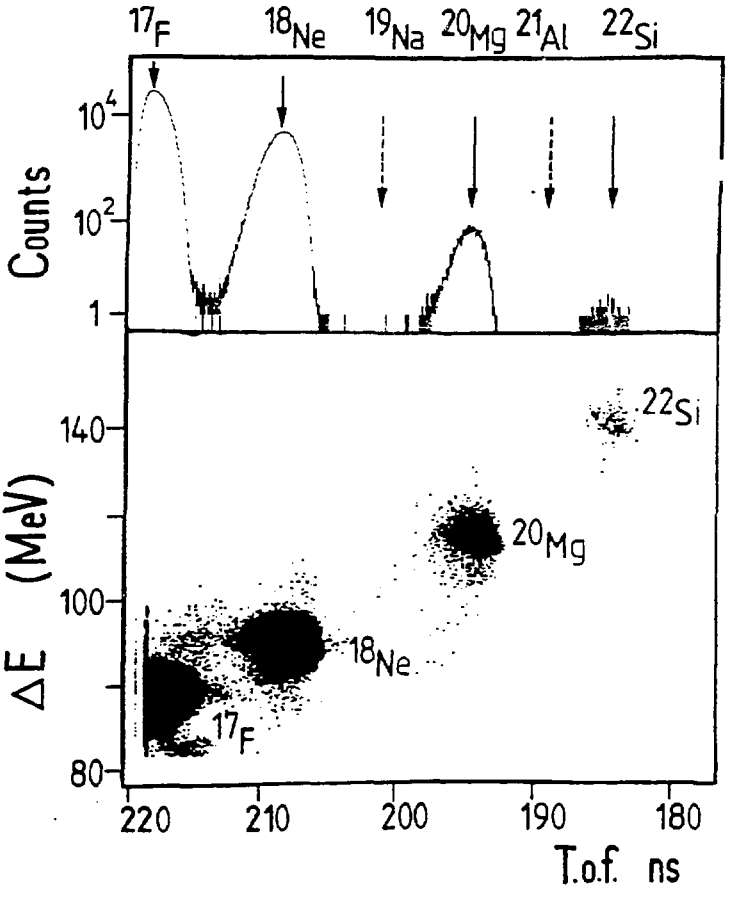
17F
18Ne
19Na
20Mg
21Al
22Si
Counts
10^4
10^2
1
ΔE (MeV)
140
100
80
22Si
20Mg
18Ne
17F
220
210
200
190
180
T.o.f. ns

Fig. 40

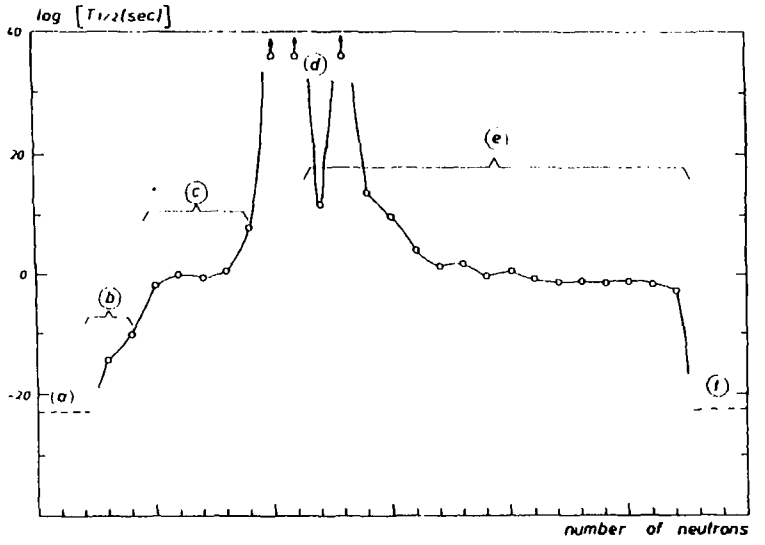

Fig. 41

Fig. 42